POLYTECHNIC UNIVERSITY OF MARCHE
FACULTY OF ENGINEERING
MASTER DEGREE IN BIOMEDICAL ENGINEERING

Dynamic Characterization of a Human Tibia Including Soft Tissues: Experimental and Numerical Analysis

Candidate:
Roberta Melchionda

Relator:
Prof. Lorenzo Scalise

Correlators:
Paolo Chiariotti
Milena Martarelli

ACADEMIC YEAR 2018/2019

Contents

Abstract

The tibia is one of the largest bones which characterize the leg. It is important for body weight supporting and for the mechanics of lower leg joints. Muscles surrounding it, through their activation, are relevant into locomotion, maintenance of posture and balance. One of the worst damages for the tibia is the fracture caused by injuries due to vehicles accident, falls, sports or disease such as osteoporosis. Fractures are classified on the basis of location, pattern and tissues damages. A simple fracture divides bone in two parts, a wedge fracture has a third segment instead the complex fracture has more than one fragments. In this last case is necessary a surgical treatment. On the basis of damages into surrounding tissues is called open or closed fracture. In case of shaft fracture, located al level of the diaphysis, is applied the external fixation, a structure characterized by pins and screws near fracture site attached to an external bar outside of skin. A subject with a tibial fracture has to undergo, during the 6 months of healing, to a high number of radiographic investigations in order to assess if there is a union, non-union or a delay in healing process. It is necessary to understand when is completed the hard bone callus formation to remove the fixation. X-rays drawbacks are the patient exposure to this dangerous rays and the high cost for the sanitary system. During the years were developed different solutions involving excitation with vibrations and measurement by accelerometer. After some improvements to avoid interference on the signal was used as, transmission medium, the external fixation. Using as starting point these studies the present work is based on the dynamic characterization of the tibia including soft tissues to highlight from FRF its mode of vibrations. The experimental test for the FRF evaluation, before fracture, is characterized by hammer excitation and accelerometer measurement both at level of the tibial shaft. From the results arise a changing for the resonant frequencies and width of the peak at which occurs the first mode for the driving point in horizontal and vertical plane, when added mass and external fixation. Furthermore is validated a numerical model of tibia including soft tissues comparing its results with the experimental ones. At the end

are observed the index healing curves in a fracture simulated by a 2 mm cut through a handsaw and the bone callus formation reproduced by a bi-component cement. During fracture simulation, the fixation is used as a transmission medium in which a pin is excited by a shaker and on the other pin is applied an accelerometer. From this last part arises that after more than one cut on the tibia and in case of adding mass there is the lack of repeatability and the healing process is not more accurate.

Introduction

The tibia is the main long bone of the lower leg which provides stability and leverage for the leg to propel a person through movements and facilitates activity of everyday life. It is fundamental for knee and ankle joint mechanics.
The most common injury is the fracture due to motor vehicles accident, falls and sports under the effect of blunt force trauma to the leg or repetitive impacts. At the same time some diseases, such as osteoporosis, could increase the possibility of stress fracture because of the bone thinning.
Tibia fractures is defined as proximal if it affects the upper part, instead "shaft" if located at level of the dyaphysis. A deeper classification is connected to the kind of fracture. Stable is a crack which leaves most of the bone in its normal position, displaced when a bone part is not aligned, spiral for the presence of a fracture spiral-shaped and comminuted when the bone is divided in more than three pieces. A fractured bone breaking through the skin causes an open fracture, in other case it is called closed fracture though there may still be internal tissue damages.
Most relevant symptoms of tibia fractures are localized pain in one area of the tibia, lower leg swelling and difficulty to stand, walk or bear weight.
In case of open fractures or with a large degree of displacement is necessary a surgical treatment. For shaft fracture the most used treatment is the external fixation. The healing process is defined as the union of the fractured components that, usually, requires around 6 months. However being able to return to normal activities it may take longer time than this. From week 6 to week 14, after the fracture, soft callus evolves in hard callus. During this period is necessary a radiographic investigation allowing the doctor to determine if the union is completed, delayed or if there is a non-union. This imaging technique is useful but at same time means a high patient's exposure to radiation and economic problem to public health because of the costs for carrying out this examination.
Over the years were developed different solutions less dangerous for the subject. The first studies are about the usage of the vibration generated by a hammer or a

shaker and an accelerometer to record signal. In recent years were introduced new technologies to overcome limitations due to direct hammering of the bone and to artefacts generated by soft tissues surrounding tibia.

A solution, in case of external fixation applied, should be represented by the excitation of one pin and the measurement at level of the pin located after shaft fracture to assess the state of healing process.

This study is based on a tibial shaft fracture in which external fixation is used as transmission medium to assess the healing and the state of union of a fractured bone including soft tissues. Adding mass, surrounding tibia, is realized in silicon because more similar to the behaviour of real situation. The first part of the work is based on the experimental tests consisting into a direct hammering of the bone in order to compare the resonant frequencies from the FRF of the tibia, tibia including soft tissues with and without fixation. Then it is realized a numerical model closer to the real one. It is validated comparing its results with what obtained from experimental part. The numerical model is important to overcome the limitation introduced by the lack of repeatability for experimental part. At the end is performed a transmissibility test using external fixation as medium for the signal generated by a shaker in the pin before fracture and recorded into the pin just after the previously. The cut for the fracture is simulated into shaft by a handsaw with a width of 2 mm and the bone callus formation is reproduced by a bi-component cement. The healing index curves obtained from experimental tests are compared with literature and are highlighted the differences between only tibia and tibia including soft tissues. As an additional proof of the results obtained are compared, also, the FRFs as a function of time and frequency recorded at level of the pin closer to fracture.

The aim of this research is the evaluation of results from experimental hammering test in presence of soft tissues, the validation of a numerical model to overcome experimental test limitations and the observation of what changes in healing index curve adding mass.

1 General concepts and the state of the art

1.1 Anatomy of the tibia

The lower leg is made of two bones: tibia and fibula. But the largest one is the tibia which supports all the body weight and plays an important role in four joints: the knee, the ankle, the superior and inferior tibiofibular joint. It has a body (or shaft), the diaphysis, and two extremities called the epiphyses (Fig.1.1). The upper extremity is large and expands in the medial and lateral condyles articulated with the condyles of the femur to form the knee joint. In the anterior surfaces the condyles are continuous and the area ends in the tibial tuberosity for the attachment of the patellar ligament; in the posterior surface the condyles are separated by a depression, the posterior intercondyloid fossa, which gives attachment to part of the posterior cruciate ligament of the knee-joint. The shaft is characterized by three borders: anterior, medial and lateral and by three surfaces which are covered by the muscle tendons. The forward flat is called fibula. The lower extremity is smaller than the upper and is prolonged downward to form a pyramidal strong process called medial malleolus. This last together with the fibula and talus of the foot forms the ankle joint. The tibiofibular joint is the formed by the articulation between the lateral side of the fibula and the lateral side of the distal tibia, called fibular notch

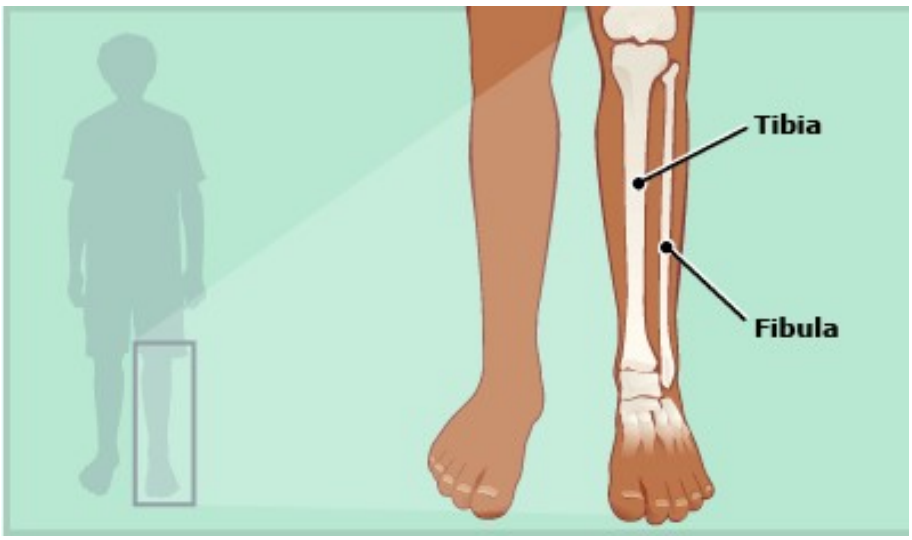

Figure 1.1: Tibia position into lower leg.

(Fig.1.2). Tibia, as the others long bones, has a hollow cavity in the middle called the "medullary cavity", filled with fat-rich yellow bone marrow that stores energy for the body. The cavity is characterized by regions of spongy bone, filling each end, and solid compact bone covering their entire structure. Spongy bone is made of tiny columns, known as trabeculae, that reinforce the ends of the bone against external stresses. Red bone marrow, which produces blood cells, is found in the holes in the spongy bone between the trabeculae. A thick layer of compact bone surrounds the medullary cavity and the spongy bone gives strength and mass to the bone. The cells which compose the compact bone are surrounded by a matrix of hard calcium mineral and collagen protein that is both extremely strong and flexible to resist stress (Fig.1.3). Periosteum, around the compact bone, is a thin layer made of a dense, fibrous connective tissue, which is continuous with the ligaments that connect the tibia to the surrounding bones and the tendons that connect the muscles to the tibia. These connections prevent the separation of the muscles and bones from each other. Finally, a thin layer of hyaline cartilage covers the ends of the tibia where it forms the knee and ankle joints. Hyaline is extremely smooth and slightly flexible, providing a smooth surface for the joint to slide across and a shock absorber to resist impacts [1].

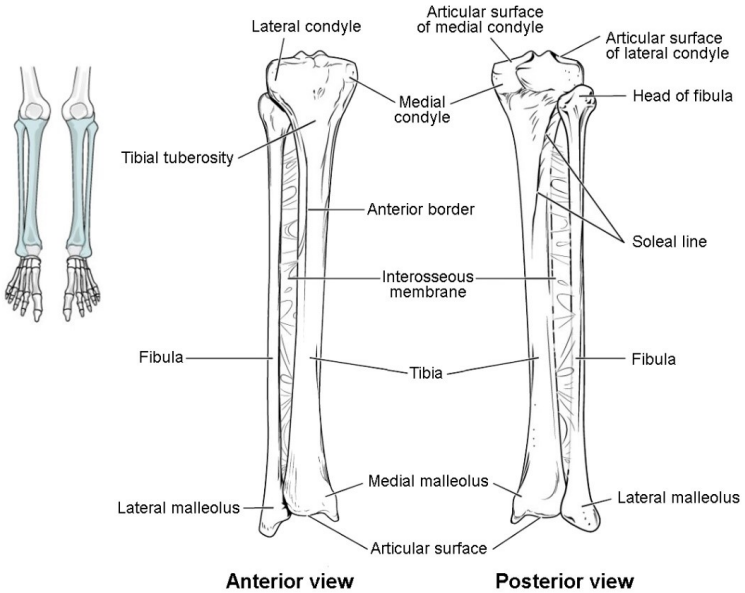

Figure 1.2: Anterior and posterior view of the tibia

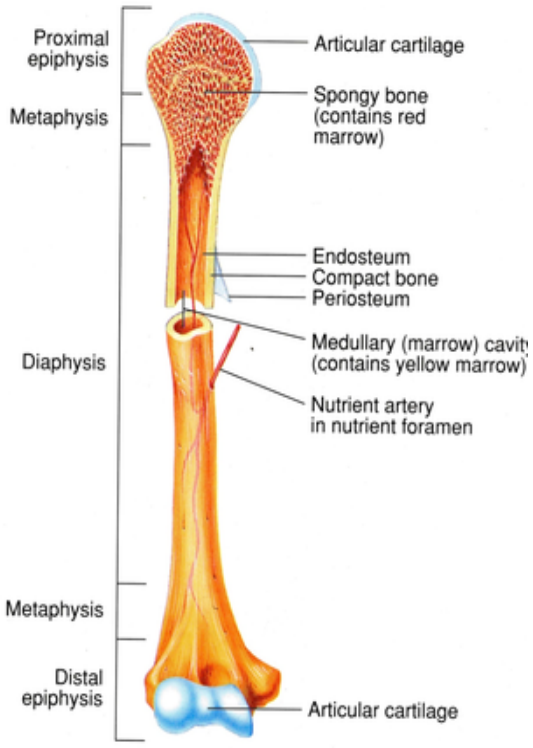

Figure 1.3: Internal structure of the tibia

1.2 Soft tissues surrounding tibia

The movement of the ankle joint is connected to variation in muscle activation and is relevant into the locomotion, maintenance of posture and balance. The lower leg muscles can be divided in three different compartments: anterior, lateral and posterior. The anterior region is composed by tibialis anterior, extensor digitorum longus and extensor hallucis longus. The posterior region is composed by gastrocnemius, plantaris, soleus and tibialis posterior. Instead the fibularis longus and fibularis brevis belong to the lateral side (Fig.1.4).

The posterior tibial artery comes from the popliteal artery and divides into two branches to supply blood to the skin, muscles and the other tissues located into the calf. The peroneal artery is the largest branch of the posterior tibial artery which travels along the fibula and is a contribute into the innervation of the ankle. The blood returning from the calf to the heart is due to the posterior tibial vein.

The tibial nerve arises from the popliteal fossa and is a branch of the sciatic nerve going towards the sural nerve. It innervates the posterolateral side of the leg, lateral

Figure 1.4: Muscles around the tibia.

side of foot and the sole of the foot. It has cutaneous and motors function in leg and foot [1].

1.3 Fracture of the tibia

A tibial fracture refers to any crack or breaks into tibia bone. The causes may be traumatic injuries as a motor vehicles accident, falls, sports which involve repeated impact to the bone or the osteoporosis which makes the bone weaker than usual. The fracture is classified on the basis of the location, of the pattern and the skin

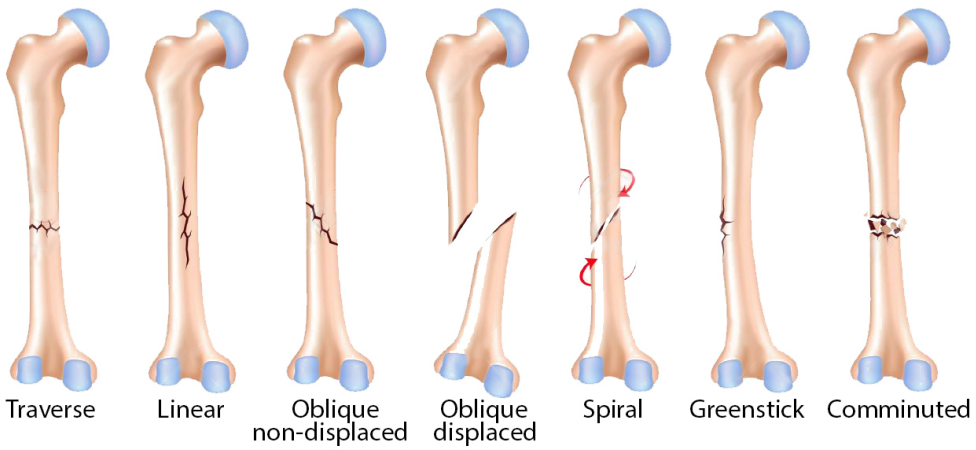

Figure 1.5: Tibial Shaft fracture.

and muscle damages. The reduction is the process of restoring the correct relation and position of fracture fragments so that the joints above and below the fracture are in correct position. A simple fracture is a single line fracture producing two fracture segments: spiral, oblique or transverse. The wedge is a fracture with a third segment, after reduction, in some way in contact with the two main fragments. The greenstick is characterized by a young, soft bone in which the bone bends and breaks. The complex (or comminuted) fracture is characterized by more than one fragments without any contact with the main two fragments after reduction (Fig.1.5). If the skin and muscle around are intact the fracture is called closed, in other case is defined as open [2],[3] (fig. 1.6). The classification of injury severity represents a

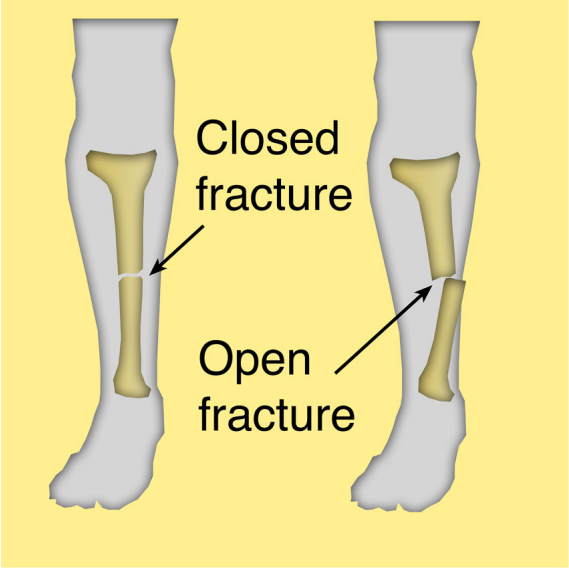

Figure 1.6: Open and closed fracture.

useful tool for treatment, outcome prediction and prognosis. In literature there are different studies for the classification of fracture on the basis of a score. In figure 1.7 are shown the parameters based on patho-anatomy of the injury used by the Orthopaedic Trauma Association (OTA) to classify open fractures in adults and paediatric long bones. Another example of open fracture classification is the one of the Ganga Hospital (fig.1.8) in which the score about skin, skeletal and soft tissues damage is between 1 and 5 [4].

Parameter		Score
Injury to skin	Small injury	1
	Large/Immeasurable injury	2
	Degloving injury	3
Muscular injury	No/Minimal injury	1
	Moderate/functional injury	2
	Extensive muscle injury	3
Arterial injury	No injury	1
	Non-ischaemic injury	2
	Ischaemia	4
Degree of contamination	No/minimal contamination	1
	Surface	2
	Deep	3
Amount of bone loss	No loss	1
	Minimal bone loss	2
	Significant bone loss	3

Figure 1.7: Open fractures classification of the Orthopaedic Trauma Association (OTA).

Parameter		Score
Skin losses	No loss	1
	Some loss/degloved *(+2 to above if over bone)*	2
	Extensive loss/exposed bone	5
Soft tissue injury	No injury	1
	Repairable	2
	Irreparable	3
	Loss of $<$2 compartments	4
	Loss of $\geqslant$2 compartments	5
Bony injury	Fracture, no bone loss	1 - 2
	Joint involvement	3
	Bone losses: $<$ 4cm	4
	$>$ 4cm	5
Additional risk factors	Age $>$65	+2 for each
	Contamination	
	Chronic illness	
	Systemic injury	
	Other trauma	

Figure 1.8: Open fractures classification of the Ganga Hospital.

1.4 Tibial fractures treatment

Open fractures and fractures with many bone fragments and a large degree of displacement need a surgical treatment. One of the methods includes the usage of **intermedullary nailing** procedure which consists into a specially designed metal inserted into the canal of the tibia in order to keep the fracture in position. The intramedullary nails are, usually, made of titanium and are screwed to both bone's ends in order to keep nail and bone into the proper position.

The tibial nailing can be used in open and closed tibial fractures and in non-union

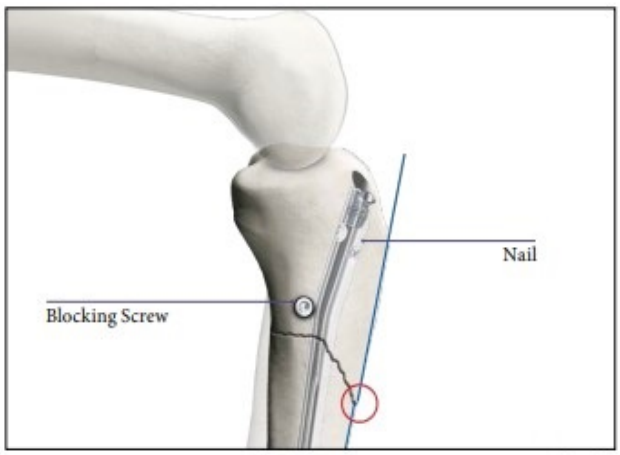

Figure 1.9: Tibial Nailing System.

and malunion condition of the bone (Fig.1.9). The risk of failure is connected to the local inflammation, the vascularity compromising, inadequate coverage tissue over the operative site, overweight of the patient that can produces loads on the implant. In order to insert the nail is necessary to create an entry point with a paratendinous incision from patella oriented in relation to the medullary canal. Additional screws make the nail more stable [5].

Another surgical solution can be the application of **external fixation** which consists in metal pins and screws, placed below and above the fracture site, attached

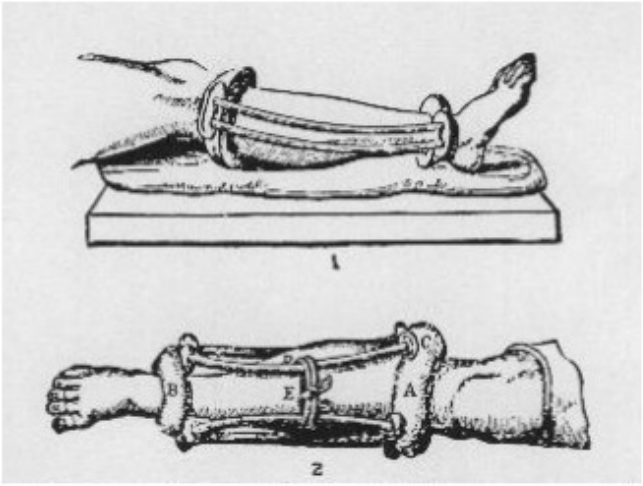

Figure 1.10: Hippocrates' external fixator.

to a bar outside of the skin.The first description of external fixator was done in 400 B.C. by Hippocrates which uses leather rings connected each other by four rods of cherry wood from knee to ankle (Fig.1.10).

The fixation, more similar to that used nowadays, were introduced at the end of 1800. The currently external fixators are an improvement of the Hoffman's model introduced in 1937 [6]. Since the external skeletal fixation are used in a high variety of application Chao and co-workers at the Mayo Clinic devised a terminology configuration (Fig.1.11). Unilateral (Fig.1.11 A) is characterized by one bar or one rod connecting two or more pin clamps. Bilateral (Fig.1.11 B) employs bars on both sides of the limb connected to pin clamps. Quadrilateral (Fig.1.11 C) uses two bars on each side of the limb, with a total of four bars. Biplanar (Fig.1.11 D) employs pins in different planes to enhance stability. Half rings (Fig.1.11 E) encircle the leg transverse to its long axis with circular half rings and uses transfixing and half-pins with

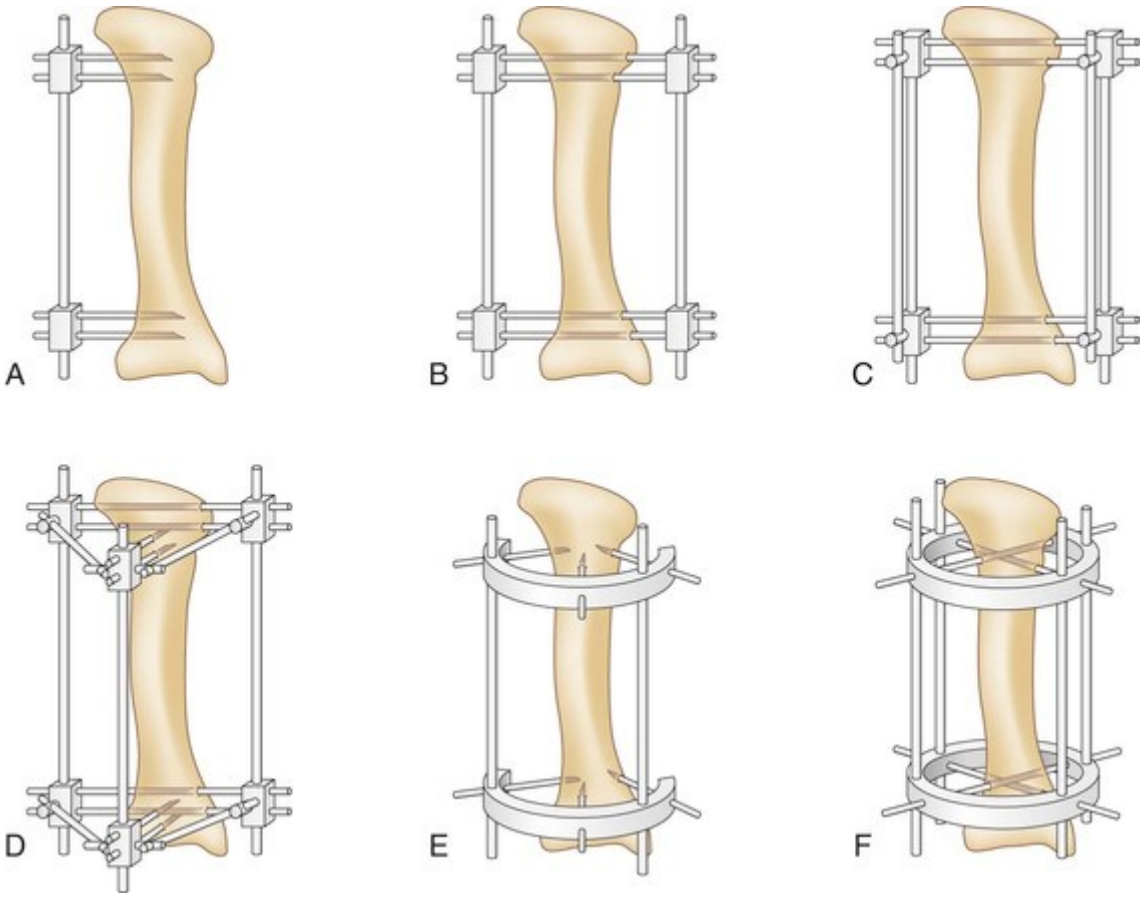

Figure 1.11: External fixator configuration.

a geometric placement dependent on the fracture. Instead ring (Fig.1.11 F) utilizes circular rings attached to the bone through transfixing rings with the possibility to increase the rigidity of the structure adding pin and rods [7][8]. One of the disadvantages in application of external fixator is the pin tract infection that can be avoided, by surgeon, following a safety procedure in a sterile operating room. The removal of external frame requires special wrenches and can be done with no anaesthesia. During application is not recommended to displace the entire muscle compartments in order to reduce the pressure necrosis of the muscle and of the overlying fat tissue. Some infection responds well to aggressive local pin care and oral antibiotics, but in other cases is better remove the pin. Green noted that to minimize the limitation of ankle dorsiflexion is necessary to dorsiflex the foot prior the application. The insertion of the pins takes place into the medial subcutaneous border of the tibia to avoid impalement of muscle tendon and nerves [8]. Raimbeau identified the susceptibility of the anterior tibial artery where crosses the lateral surface to the tibia, thanks to his studies conducted on cadavers [9]. X-ray imaging technique provides clear images able to estimate whether the tibia is broken or intact, where is located the fracture, what kind of fracture affects the bone and whether knee, ankle joints or the fibula are involved. Usually, most tibial shaft fractures take 4 or 6 months to heal completely during which is necessary the physical therapy to restore normal muscle strength, joint motion and flexibility. Further studies are necessary to find methods for the evaluation of the degree of healing reducing patient exposure to the X-ray.

1.5 The state of the art

Over the years were developed different solution to solve the problem of the X-rays patient exposure to check the phase of the healing process.

The first and real application of the impulse response method to determine the mechanical properties of the fractured bone was done in 1932 by Lippmann. The bone was percussed with a finger and the measurement done with a stethoscope. The fracture classification was based on the changing in response pitch and quality; in case of poor conduction, due to bad contact, the sound is reduced. This application reduces the exposure to the X rays and is very simple, immediate and accurate [10]. In 1942 McGaw [11] continued to use the percussion-auscultation method.

During the following years Sekiguchi and Hirayama [12] used a tapper to strike the medial malleolus (Fig.1.12) in order to generate percussion note (p-note) transformed into the analysed waveform. Vibrations are within the audible range (20-20000 Hz) under hypothesis that bone dynamics changes for fracture and during healing progression. The measurement is done by a piezoelectric sensor connected to a preamplifier and with results visible into a display. The 41 cases of fresh fracture are classified as:

- type 1 (one cycle wave);
- type 2 (two or three cycle wave);
- type 3 (four or five cycle wave);

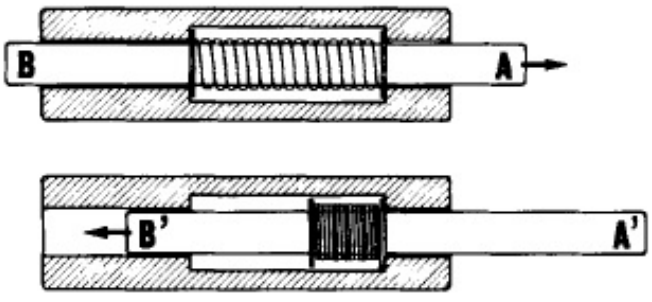

Figure 1.12: Tapper.

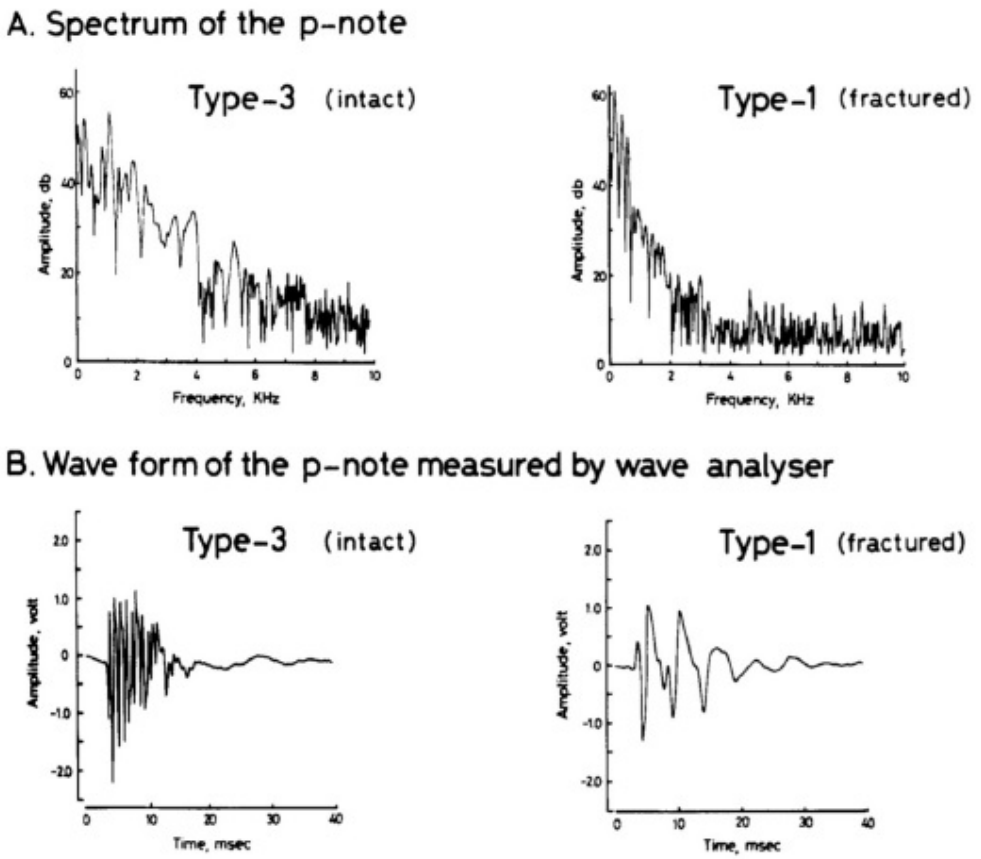

Figure 1.13: Example of percussion note in intact and fractured bone.

The results show how the waveform with time become more similar to the intact bone. Into figure 1.13 is highlighted the difference of classification. This test is more sensitive than the X-rays method in assessing pathological situation as a delayed healing process. In case of delayed or pathology fracture the wave does not improve in time. Instead the effect of the fibula could be defined as negligible. In figure 1.14 is shown the waveform of the fractured bone becomes equal to the normal one. It passes from pathological type 1, to type 2 which corresponds to roentgenographic union and at the end in type 3 that is union.

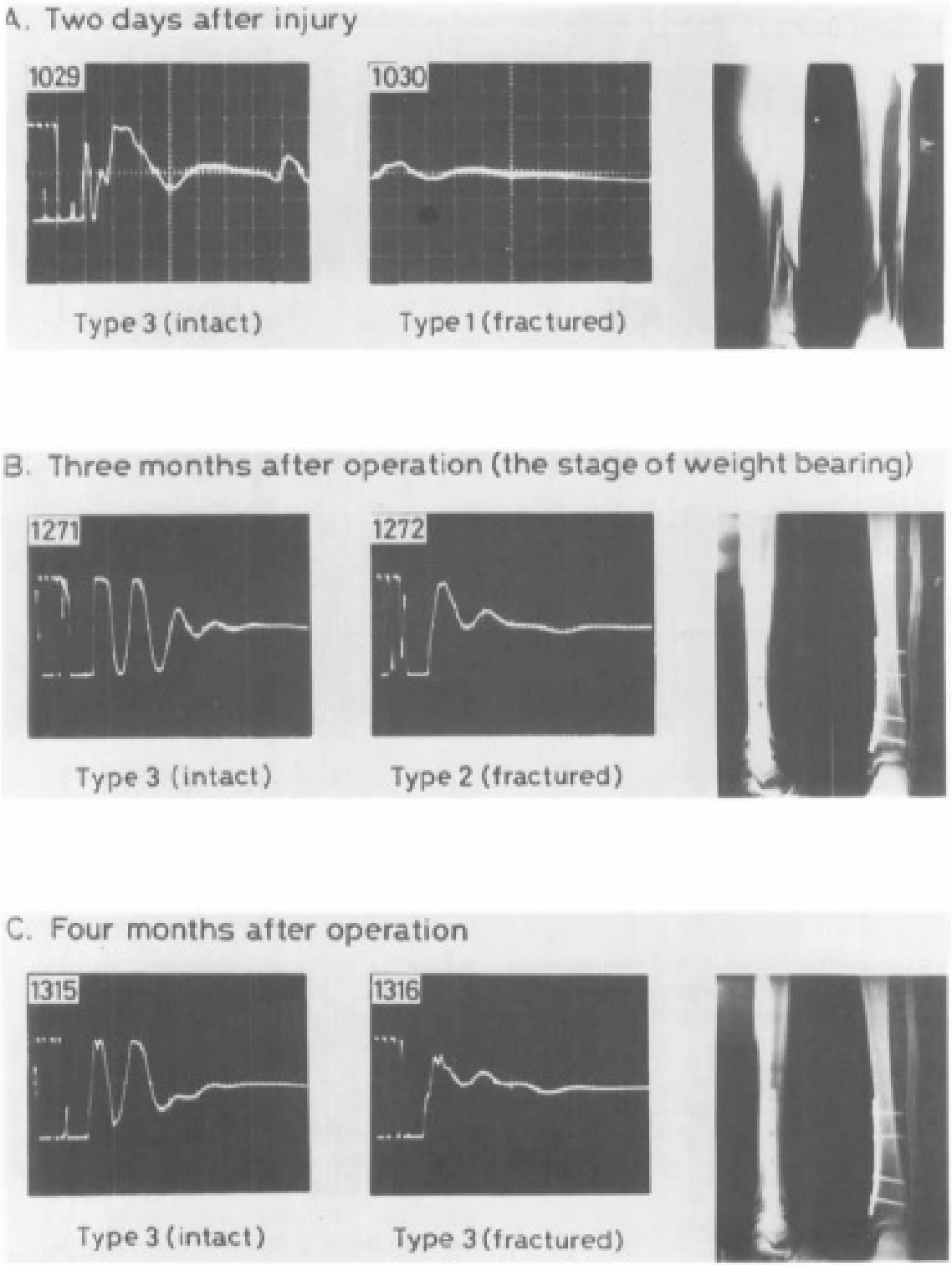

Figure 1.14: Stages from fractured to healed bone.

In 1986 Cornelissen and Van der Perre [13] analysed the influence of soft tissue, joints and fibula on the vibration of the human tibia by modal analysis on cadaveric

Figure 1.15: Impulse frequency response configuration.

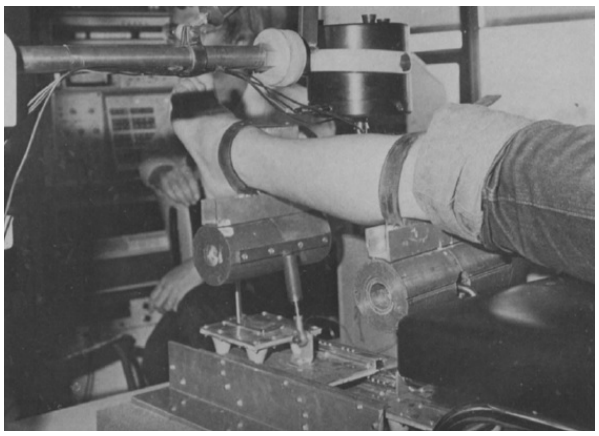

Figure 1.16: Bone Resonance analysis.

bones. The two setups for the measurement are the IFR (Impulse Frequency Response), based on the excitation with a hammer and accelerometer manually pressed against the bone to measure, and the BRA (Bone Resonance Analysis) with the usage of an electromagnetic shaker (Fig. 1.15 and 1.16). Without some specimens the damped resonant frequencies increase and the damping ratio decreases. In the IFR configuration the hanging leg reproduces the free-free condition, for this reason joints do not influence a lot. The bending modes are identified at 350 and 550 Hz. Instead into the other configuration is not possible to determine the joints as the blockage following disarticulation. The bending modes arise near the previously but with another one around 160 Hz.

In both cases the skin removing is not influential in modal parameters, but could limit the frequency range (Fig. 1.17). At the same time the muscles change the resonant frequencies and act as a damper material (Fig. 1.18 and 1.19). The fibula produces a stiffening effect.

Specimen conditions	Mode 1 f_d (Hz)	Mode 1 ζ (%)	Mode 1 α (degrees)	Mode 2 f_d (Hz)	Mode 2 ζ (%)	Mode 2 α (degrees)
A1	347	21	90	513	10	0
A2	351	19	90	524	12	0
A3	386	15	+60	540	9	−30
A4	391	16	90	568	7	0
A5	392	10	90	570	7	0
A6	394	8	90	572	7	0

f_d: damped natural frequency (Hz).
δ: damped ratio (% of critical damping).
α: orientation angle of mode (see also Fig. 2).
$\alpha = 0°$: anterior direction.
$\alpha = 90°$: medial.
$\alpha = -90°$: lateral.

Figure 1.17: Results from IFR configuration.

- A1: intact;
- A2: after stripping of the skin along the medial face and the anterior border;
- A3: after removal of the anterior muscle group;
- A4: after removal of all other muscles;
- A5: after exarticulation in the ankle joint;
- A6: after exarticulation in the knee joint: tibia+fibula in excised state;

Number of test	Mode 1 f_d (Hz)	Mode 1 ζ (%)	Mode 1 α (degrees)	Mode 2 f_d (Hz)	Mode 2 ζ (%)	Mode 2 α (degrees)	Mode 3 f_d (Hz)	Mode 3 ζ (%)	Mode 3 α (degrees)
B1	168	33	15	303	20.3	75	470	13	0
B8	—	—	—	363	5.2	90	512	4	0
B2	160	19	0	287	21	−60	342	21	15
B3	154	19	30	270	23	−45	348	17	0
B4	147	19	45	243	22	−90	335	26	0
B5	158	17	45	260	20	−45	360	15	−15
B6	155	19	30	260	19	−30	370	14	30
B7	156	18	0	263	17	−60	377	11	30

f_d: damped natural frequency (Hz).
δ: damping ratio (% of critical damping).
α: modal orientation (see also Fig. 2).
$\alpha = 0°$: anterior.
$\alpha = 90°$: medial.
$\alpha = -90°$: lateral.
$\alpha = 180°$: posterior.

Figure 1.18: Results from BRA configuration.

Number	Specimen condition	Supporting condition	Excitation
B1	Intact	Hanging free	Hammer impact
B2	Intact	Supported	Hammer impact
B3	Skin stripped along medial face and anterior border	Supported	Hammer impact
B4	Fibula osteotomy	Supported	Hammer impact
B5	Removal of anterior muscle group	Supported	Hammer impact
B6	Removal of peroneus muscle group + superficial of posterior muscle group	Supported	Hammer impact
B7	Removal of fibula + all other muscles	Supported	Hammer impact
B8	Excised tibia	Free-free	Hammer impact

Figure 1.19: Procedure for the BRA test.

Starting from the previously results, Tsuchikane and Nakatsuchi [14] studied in vivo the vibrational response of the tibia surrounded by soft tissue. Their aim is to apply and detect an accurate signal and to clarify the influence of soft tissues on the vibrational mode. This study is done on cadaveric human leg and divided in different experiments to understand the influence of skin, muscles and joints. The location of the impulse hammer was the medial malleolus instead the accelerometer was on the medial condyle. The input and output signal were connected to a two-channel charge amplifier and processed by a fast Fourier transform analyser

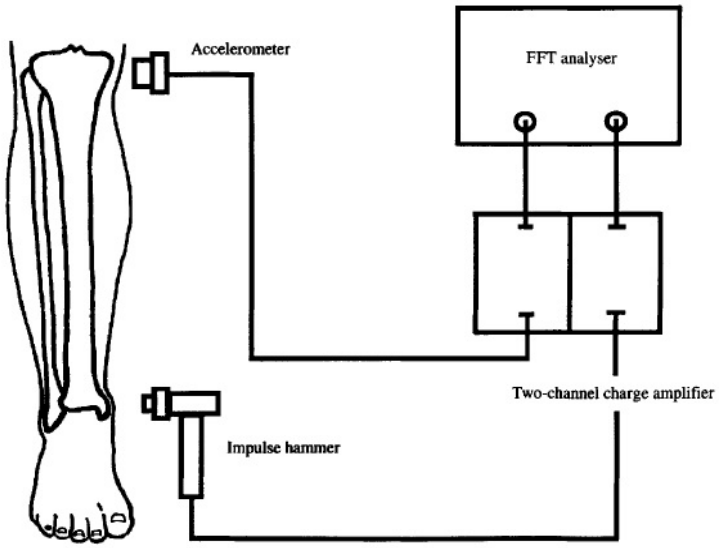

Figure 1.20: Experimental setup.

to analyse the resonant frequency (Fig.1.20). It was observed that the removal of the muscles causes a high decreasing into the weight. The results, in case of skin absence, shows not relevant effect on modal parameters. The muscles and foot are the most relevant vibrations absorbers, but also the skin, soft tissue, joints and fibula contribute to increase the damping effect and the "apparent" weight. So, as the adjacent structures are removed from the tibia, the result is a lower value of the damping ratio as shown into the figure 1.21. For what concern the resonant frequencies it is possible to see into the figure 1.22 that the value increases with the removal of the skin, muscles and foot, but decreases with the removal of the femur and the fibula. Another important conclusion is that the bending mode and

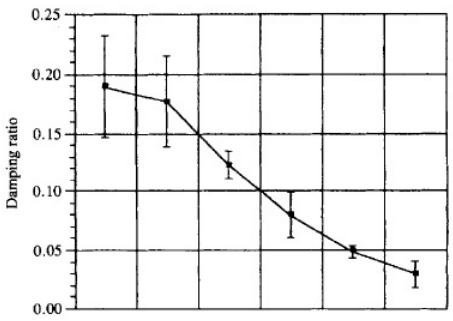

Figure 1.21: Damping ratio.

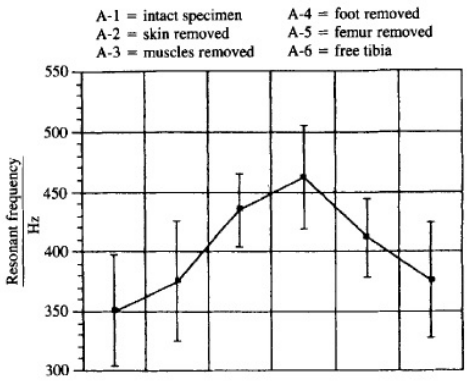

Figure 1.22: Resonant frequencies.

its mode shape are not influenced by the joints, so any change in resonant frequency is due to the tibia itself. This study represents an important starting point to evaluate the mechanical properties of a tibia which is surrounded by the adjacent soft tissues and confirms what obtained into the Cornelissen and Van der Perre work [13].

Ong et al.[15] work is based on an integrating SHM concepts into external fixation to asses the state of healing process in a fractured femur. The fracture is realized by cut and filled with epoxy to simulate the healing. The external fixation used is a Hoffmann II MRI (Fig. 1.23) that is undergone to a finite element analysis to study its behaviour. Instead the soft tissues is simulated by clay (Fig.1.24). A solenoid impactor with a load cell is applied to the femur, instead a polyvinylidene

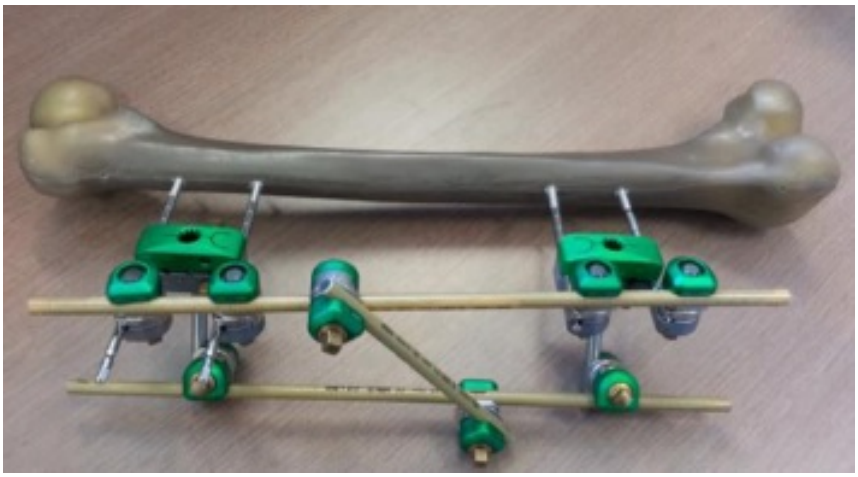

Figure 1.23: Model tibia with Hoffmann II external fixation.

Figure 1.24: Tibia surrounded by clay to simulate the soft tissues.

fluoride (PVDF) film sensor is located in the pin of the fixation. Two kind of adhesives are inserted in order to simulate non-union or delayed union. The differences into the transfer function means an increasing into the stiffness and the evaluation of a healing index. The inspection of the gradient, starting from the healing index data, allows to derive the state of union. However are necessary additional methods to assess time returning to normal activity.

Mattei et al. (2017) [16] used a frequency response analysis for the healing assessment in case of treatment with external fixation. They used a 4th generation Sawbones tibia model with a Hoffmann 3 Stryker fixation (Fig. 1.25). Both the excitation and the measurement are done at level of the fixation pins to overcome the limitation in excitation through the soft tissues. The specimens, undergone the test, are a tibia phantom, a tibia phantom with pins and a tibia phantom with an external fixation (Fig.1.26). The excitation is realized with a micro-hammer, a hammer and an electromagnetic shaker, but the better device to be used is the micro-hammer because more handle and gentle (Fig. 1.27). The pins chosen in the test are the two (S2 and S3) respectively before and after the bone fracture in order a signal with grater Signal to Noise Ratio (SNR) (Fig.1.25). The measurement is done by a 3D accelerometer and the test is performed by the LMS Test.Lab by Siemens.

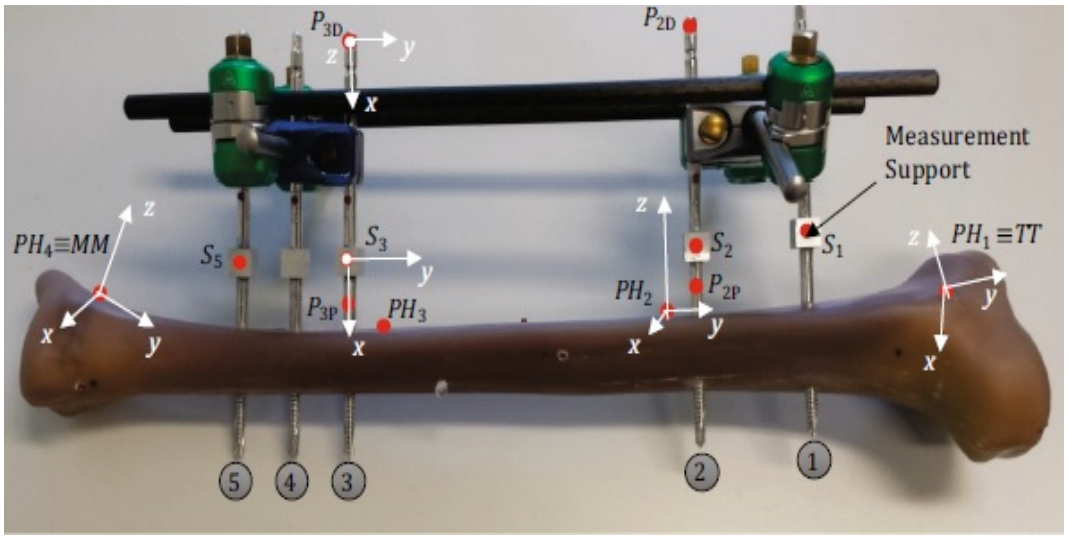

Figure 1.25: Tibia with the whole fixation.

Figure 1.26: Specimens used. (a) phantom tibia, (b) phantom tibia with pins, (c) phantom with fixation.

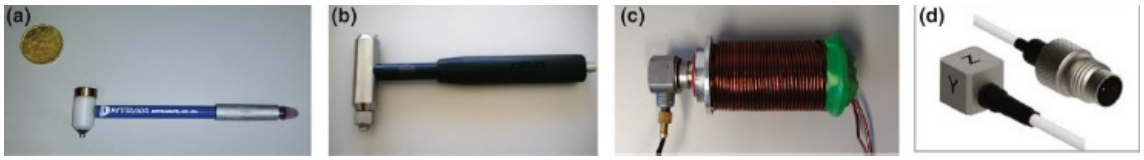

Figure 1.27: Excitation. (a) micro-hammer, (b) hammer, (c) shaker, (d) 3D accelerometer.

The data obtained are the power spectral density, the FRFs, the coherence and the resonant frequencies through the Polymax fitting tool. The system characterized by the pins and by the fixation generate a more complex vibrational response with a higher number of modes, because it introduces a complex anisotropic stiffness. However, all the three FRFs can be used to observe the changing of the frequencies during the healing process. The disassembly-reassembly of the system did not influence the results of the vibrational test, confirming test repeatability. So, the fixation can be defined a good choice as input for the assessment of the healing process.

In 2018, Mattei et al. [17], applied the results obtained from the previously study in in vivo conditions to assess bone healing of a fractured tibia treated with external fixation through resonant frequency. The linearity and quality of the system are estimated by reciprocity and coherence. The experimental setup included the usage of a micro-hammer for the excitation, a 3D accelerometer for the measurement and the LMS TestLab Software by Siemens for the data acquisition (Fig.1.28). From the Frequency Response Function are extracted the Resonant Frequencies through fitting algorithms called Polymax Plus. As expected, the results of the resonant frequencies associated to the different configurations (C1, C2: tibia with fixator and C3: tibia with only pins) were not comparable. The increasing of the first frequency, before callus formation (weeks 6-9-11), is of 4% per week instead, after hard callus

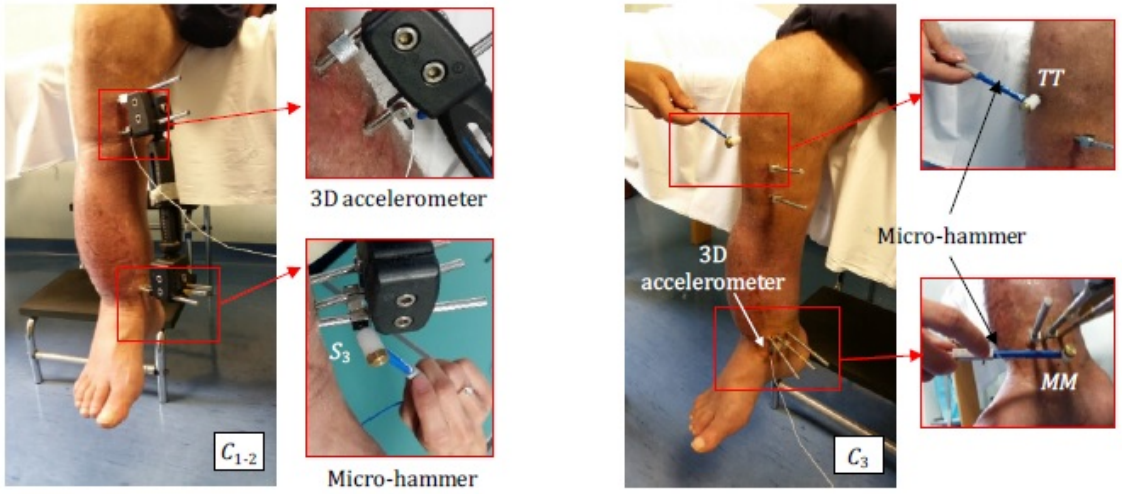

Figure 1.28: Experimental input-output.

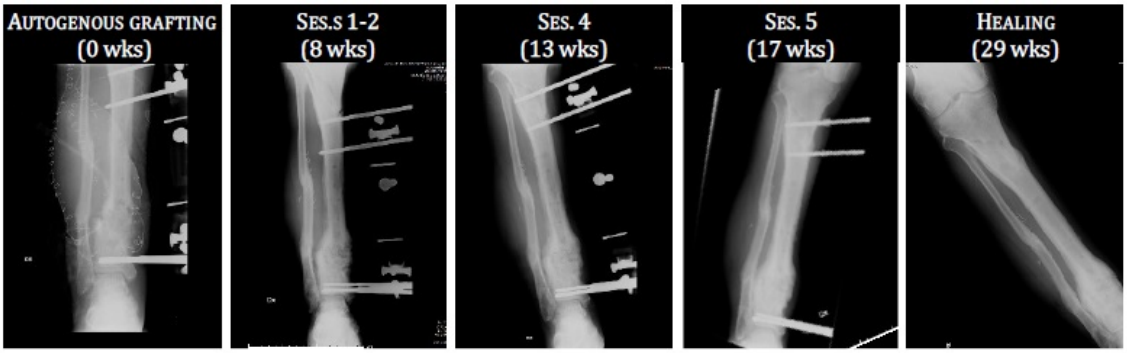

Figure 1.29: X-rays results to compare with the experimental test.

formation (weeks 13-17) the other frequencies increase of the 6% per week. This result is in line with what obtained through the X-rays (Fig.1.29), but further studies are necessary in order to widen the dataset and improve the statistical significance.

Verdenelli et al. [18] study is based on the numerical and experimental characterization of the tibia with and without the external fixation. Free-free boundary conditions are simulated by a foam support. The aim is to understand what is the best input/output configuration that can be used for the measurement and to validate a 3D model to predict the behaviour with all the external fixation configuration for the fracture treatment. The influence of the external fixation applied to the tibia when subjected to vibrations is a block of the second vertical mode and a shift downward of the second and third horizontal mode. The results, compared with Mattei et

al. [16] work, confirm that the best input/output is characterized by the shaker and the accelerometer. Shaker allows the repeatability and an amount of energy higher than that of the micro-hammer. There are few differences, in comparison with the other study, due to the presence of the stinger for the connection between the shaker and the tibia and to the location of the excitation respect the bone malleolus.

As confirmed by different studies the vibrational test can be used as a valid test to understand the healing process of the fractured tibia treated with external fixation.
This study analyses the effect of soft tissues, surrounding tibia, using the experimental setup of Mattei et al. and observing the FRFs. Furthermore is realized a numerical model of the tibia surrounded by tissues to study the behaviour and are evaluated the healing index curves.

2 Experimental dynamic characterization

In everyday life the tibia carries body weight and is undergone to a lot of stress due to activity as walking or simply maintaining erect posture. The dynamical characterization is important to understand the impact in physical activity of the fracture and what happens during the healing process. The following chapter will describe the Experimental Modal Test, in order to compare the results of the tests between the tibia, the tibia surrounded by the soft tissues and the tibia with soft tissues and external fixation applied, both in case of healthy and fractured bone.

2.1 Tibia model surrounded by soft tissue

The two tibia models used for the experiment are 4th generation Sawbones large left tibia (#3402) (Fig. 2.1). The weight is around 350 g, the length is 400 mm and the diameter of the inner canal is 10 mm. This model is made of a composite material to reproduce the real bone, with the cortical bone of short fiber filled epoxy (Young's modulus between 10-16 GPa) and the cancellous bone of rigid polyurethane foam (Young's modulus between 137-155 MPa). In order to realize the tibia model surrounded by muscles and soft tissues, a mono-component acetic silicon sealant was used, because more similar to the real stiffness and elasticity. At first was realized a hollow cast made of orthopaedic plaster to reproduce the real soft tissue surrounding the bone (Fig.2.2a and 2.2b). Then this cast is inserted at the centre of a wooden box which was filled with plaster in one half (Fig.2.3).

Figure 2.1: Tibia Model.

(a) Frontal view. (b) Lateral view.

Figure 2.2: Orthopaedic plaster.

Once dried there was the plaster casting of the remaining part of the box. The plaster cast was opened and the orthopaedic plaster was removed. The tibia was inserted into the plaster cast in a position similar to that of real bone (Fig.2.4) and there was the silicon casting in order to reproduce the tibia with the surrounding soft tissues. The amount of silicon around the tibia was of 2 kg; for this reason, was necessary to wait two weeks before starting the experimental tests on the model (Fig. 2.5a). The second tibia was undergone the same process with the only difference that into the cast were drilled holes to the following insertion of the pins belonging to the external fixation (Fig.2.5b). The dynamic characterization of the tibia is done by an Experimental Modal Analysis (EMA). The input/output configuration used for the first part of the test is composed by an excitation with a micro-hammer and the measurement with a monoaxial accelerometer.

Figure 2.3: Wooden box in which is inserted the plaster model.

Figure 2.4: Plaster cast with the tibia inserted before the silicon filling.

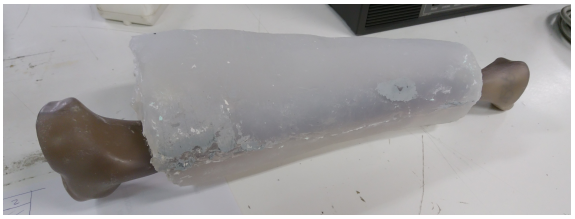

(a) Tibia.

(b) Tibia with pins.

Figure 2.5: Tibia with silicon.

2.1.1 Input excitation

The tibia model is excited by a micro-hammer with the setup shown into the figure 2.6. The model chosen in this study is a Modally Tuned ICP® Impulse Hammer by PCB Piezotronics (Model No: 086D80) (Fig. 2.7a). The tip used, according to model characteristic, is the one in vinyl with a sensitivity of 15.92 mV/N and a resonant frequency $\geq$100 kHz. The device works parallel to a PCB ICP® Power Unit (Model No: 484B) (Fig.2.7b) which has an AC signal decoupling mode for standard operation with ICP® systems and a DC mode for the calibration or ultra low frequency operation. It can supply from 2mA to 20 mA constant current to ICP® transducer or amplifier [19].

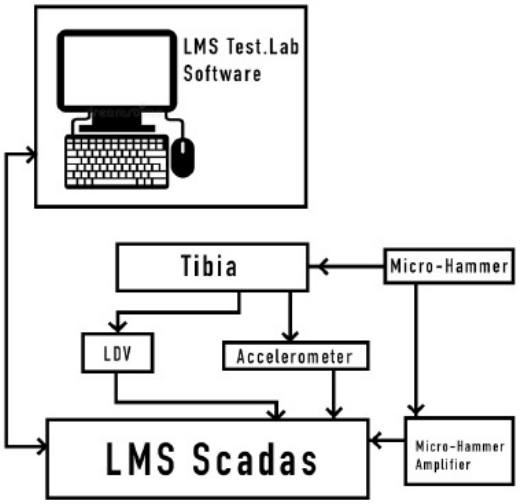

Figure 2.6: Dataset of the impact test.

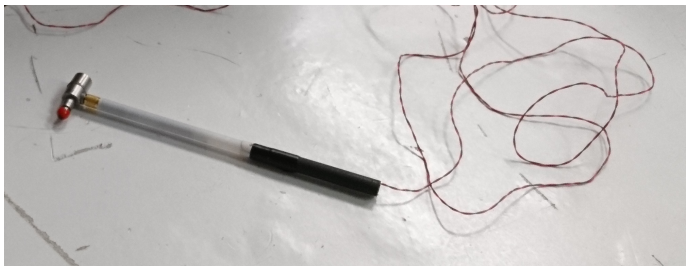

(a) Micro-hammer.

(b) PCB Power unit.

Figure 2.7: Components for the impact test.

2.1.2 Output measurement

The output is measured by a mono-axial PCB ICP® accelerometer (Model No: 352C23) (Fig.2.8). This device has a low sensitivity of 5.22 mV/g, low impedance output signal, low noise and intrinsic self-test feature. The resonant frequency is ≥70 kHz and the optimal frequency range (+/- 5 %) is between 2.0 and 10,000 Hz. The power source are constant current conditioners from 2 to 20 mA and the output impedance is ≤200 Ohm. The size of the device is of 2.8 mm [20]. The choice of the mono axial accelerometer is done because it does not influence the dynamical

Figure 2.8: Monoaxial accelerometer [20].

response of the lightweight structure. In order to attach the device on the tibia, reducing the damping effect, is applied a little quantity of wax.

2.1.3 Free-free boundary conditions

The free-free boundary conditions are reproduced by two acoustic foam located near the lower and upper epiphyses of the tibia (Fig.2.9). The same is done with the tibia surrounded by the silicon, but in this case the two foams are located on a support (Fig.2.10).

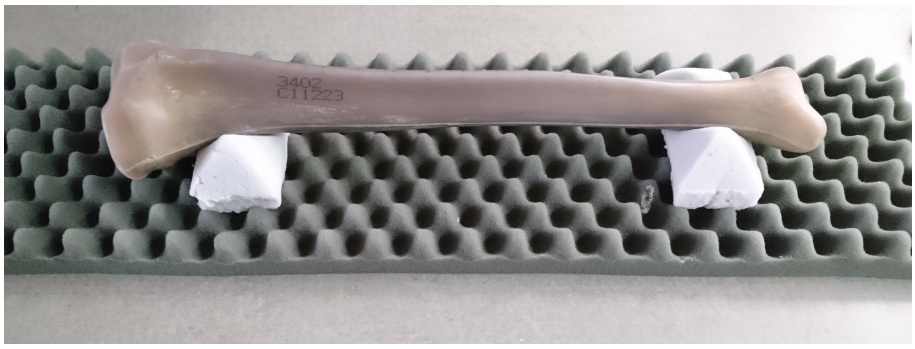

Figure 2.9: Free-free boundary condition for the tibia model.

Figure 2.10: Free-free boundary condition for the tibia surrounded by silicon.

2.1.4 Signal analysis

The experimental vibration analysis was done with the LMS Test.Lab by Siemens which includes tools for the data acquisition (LMS SCADAS), test execution and data processing (LMS Test.Lab Software) (Fig.2.11).

The LMS SCADAS acquires both from the load cell and the accelerometer and

Figure 2.11: LMS SCADAS.

controls, through a digital-analog converter output, the amplifier connected to the micro-hammer and the shaker. The LMS Test.Lab Software is characterized by different modules. The impact testing and the impact spectral enable an easier test execution for the hammer and shaker test. The modal analysis module identifies the dynamic properties in order to create Frequency Response Function (FRF), perform modal parameter estimations, validate the experimental modal analysis modes and compare original and synthesized FRF results. The resonant frequencies are evaluated by the Polymax curve fitting tool and there is the possibility to show and visualize in conjunction with the geometry of the resultant model vibrating modes [21].

2.2 Tibia with external fixation

In one of the two tibia, surrounded by silicon, was applied the external fixation in order to compare the results. The configuration followed is the standard one used for the tibial shaft fracture treatment. The external fixation used in this study was a Hoffmann II Tibia Shaft Frame. The weight is around 677.04 g. Into the figure 2.12 are shown the principle components of the external fixation. The fixation's pins are made of austenitic steel; the clamps, the couplings and posts of aluminium;

Figure 2.12: Principle components of the Hoffmann II Tibia Shaft Frame external fixation.

instead the connecting rods of carbon fibers. The component in direct contact with the bone are the pins [22].

2.2.1 Input excitation

One of the pins of the external fixator is excited with vibration exciters (called also shakers) provided by permanent magnets which are portable and stationary systems to reproduce environmental effects. This kind of excitation allows to obtain results better than that with the micro-hammer. Into the figure 2.13 is shown the experimental setup. The model used is a Tira GmbH (type: TV 50009)(Fig. 2.14) characterized by a high lateral and axial stiffness (Fig.2.15). The device is powered by a power amplifier BAA 60 which can control test systems with a maximum of 60 VA (Fig. 2.16). Into the figure 2.17 are written the technical specification [23]. The shaker excites lateral condyle of the tibia in an oblique way respect the horizontal plane in order to excite both the horizontal and vertical bending modes. The connection with the model is realized through a stinger of 7 cm in length and a PCB dynamic force sensor (208 A03) to record the force generated (Fig.2.18).

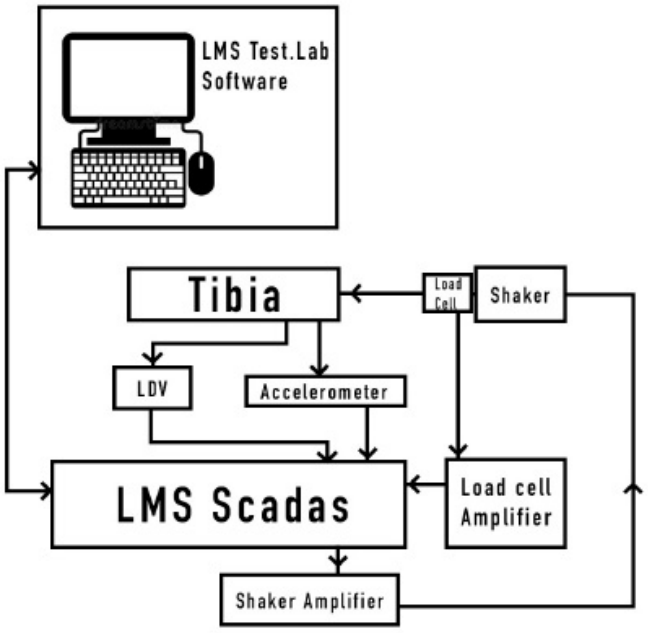

Figure 2.13: Shaker setup.

Figure 2.14: Vibration exciter.

Rated peak force $Sine_{pk}$	9 N
Frequency range	2-20000 Hz
Main resonance frequency	>13000 Hz
Max. displacement Peak-Peak	3 mm
Max. velocity Sine	1.5 m/s
Max. acceleration Sine	60 g
Suspension stiffness	4 N/mm
Effective moving mass	0.015 kg
Weight without/with trunnion	1.7 kg / 2.2 kg
Armature coupling thread size	M4

Figure 2.15: Parameters [23].

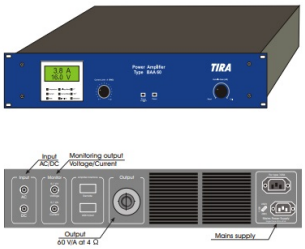

Figure 2.16: Power amplifier BAA 60.

Rated peak force $Sine_{pk}$	9 N
Frequency range	2-20000 Hz
Main resonance frequency	>13000 Hz
Max. displacement Peak-Peak	3 mm
Max. velocity Sine	1.5 m/s
Max. acceleration Sine	60 g
Suspension stiffness	4 N/mm
Effective moving mass	0.015 kg
Weight without/with trunnion	1.7 kg / 2.2 kg
Armature coupling thread size	M4

Figure 2.17: Technical specification [23].

2.2.2 Output measurement

The output of the experimental test is measured, as the previously case, with a monoaxial accelerometer applied to the second pin closer to the fracture region.

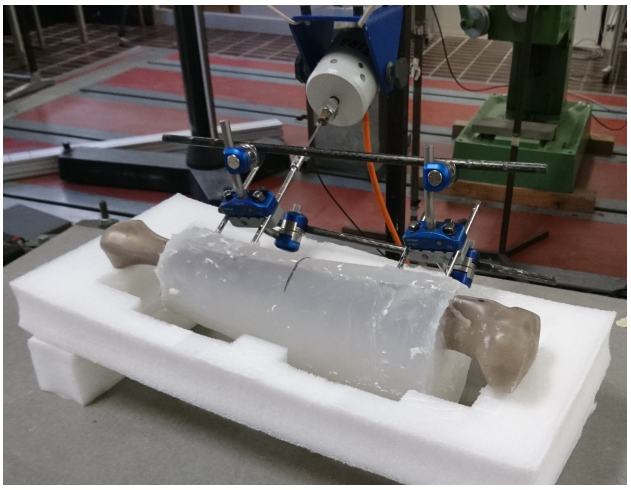

Figure 2.18: Shaker excitation of one pin of the external fixation.

Also, in this case to reduce the damping effect the device is applied through wax (Fig.2.19). In this case the boundary conditions are reproduced through a foam support opened into the inferior part in order to recreate the same condition of the previously experiment in which the only contact is with the two epiphyses.

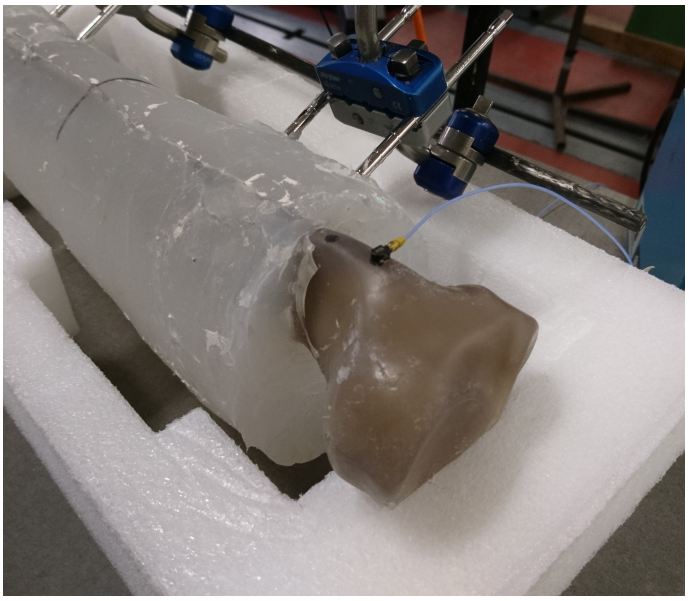

Figure 2.19: Mono axial accelerometer applied on the tibia with external fixation.

3 Numerical model

This chapter will explain how to obtain a faithful numerical model, able to predict and to observe the system behaviour. This kind of model is preferred because of its generality for what concern variable properties, arbitrary geometry, boundary conditions and processes.

3.1 Numerical model of tibia surrounded by soft tissues

The Finite Element Analysis (FEA) is the application of the Finite Element Method (FEM) to predict and to understand the behaviour of physical systems such as deformation of solids, heat conduction and fluid flow.
The body under study is subdivided into an assembly of small parts called "finite elements" for their limited number of degrees of freedom used to model the behaviour of each single element. This step is known as discretization. The elements are supposed to be interconnected into the "nodes" situated on their boundaries. The state of displacement within each finite element is described by a set of functions. The assemblage of the nodes is called "mesh".
FEM procedure calculates approximated solutions to the partial differential equations (PDEs). The aim is to transform the differential equations into a set of linear equations which can be solved by computer [24].
COMSOL Multiphysics is a cross-platform finite element analysis, solver and multiphysics simulation software. It allows conventional physics-based user interfaces and coupled systems of PDEs.
The 3D model of the tibia used is the same of Verdenelli study [18], obtained as a scan through the Non-Contact 3D Digitizer-RANGE 7 by KONICA MINOLTA. The tibia was placed on a table and covered by a powder spray in order to have a reflective surface. The two scanned tibia halves were merged using the 3D Scanning System Software and then the model was undergone to a refinement process for the mesh through the Meshmixer.
The soft tissues, silicon surrounding the tibia , is realized in Solid Edge as a "loft" of six ellipses measured from the real model (fig. 3.1). The 3D tibia and soft tissues

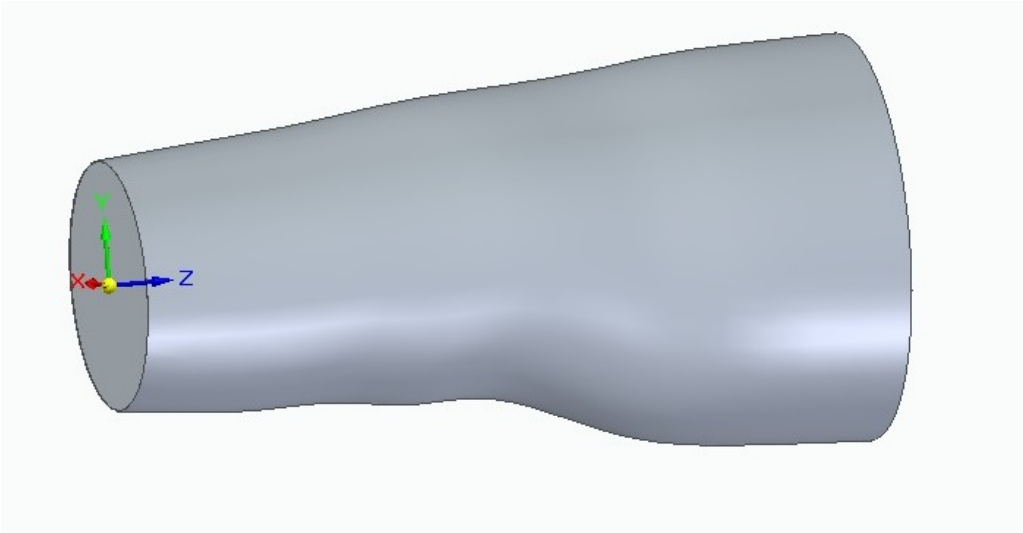

Figure 3.1: Soft tissues 3D model in Solid Edge.

models were both imported in COMSOL and moved to assume a system similar to the real one. The simulation was done into the Structural Mechanics Module. At first there was a difference between silicon and tibia model and then an union to reproduce them as an entire rigid body (Fig. 3.2 and 3.3). Into the geometry section were inserted the points used for the excitation and for the reproduction of the boundary conditions.

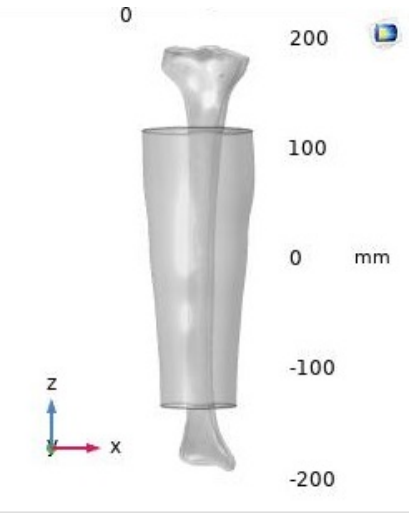

Figure 3.2: ZX view of the model.

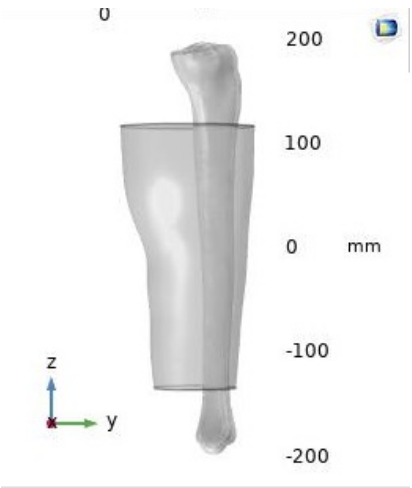

Figure 3.3: YZ view of the model.

Then were inserted the materials of the model:

- Filled epoxy resin (X238) simulating the cortical bone(Elastic Modulus 13 GPa, Density 1640 kg/m^3, Poisson ratio 0.4);
- Polyurethane (solid) simulating the cancellous bone (Elastic Modulus 155 MPa, Density 270 kg/m^3, Poisson ratio 0.4)
- Silicon simulating the surrounding soft tissue (Elastic Modulus 200 MPa, Density 905.2 kg/m^3, Poisson ratio 0.28)

The Young modulus of the silicon was found, identifying at first the range of interest between 160 and 280 MPa. Comparing the results obtained from modal analysis in Comsol, the values closer to what we want is around 200 MPa. The density was found as ratio between mass and volume directly evaluated in Comsol for the silicon domain.
In the Structure Mechanics Module was selected the point load for the harmonic perturbation simulating the hammer impact in two different axis for the horizontal (Fig. 3.4) and vertical plane (Fig. 3.5).

There were inserted also the four points simulating the contact between the model and the acoustic foam. It was inserted a mesh finer to the entire model.

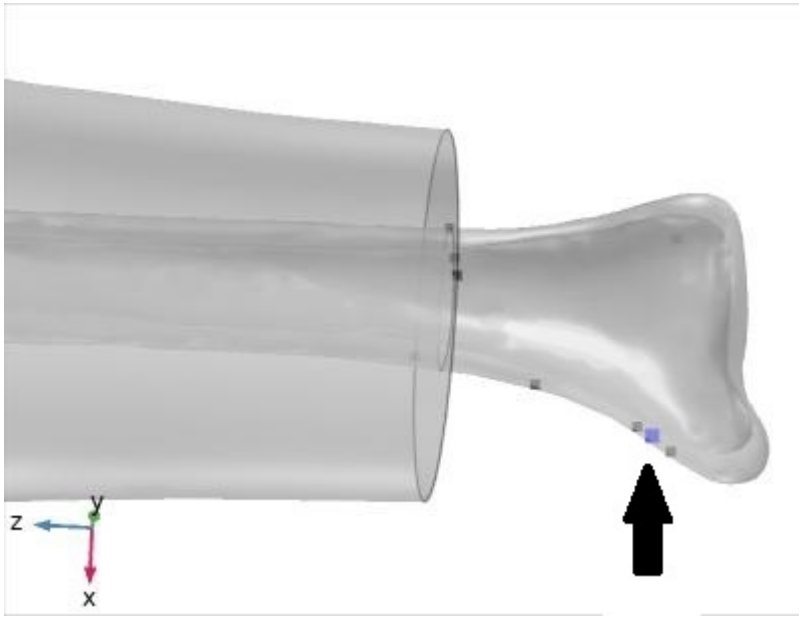

Figure 3.4: Point load for the horizontal plane.

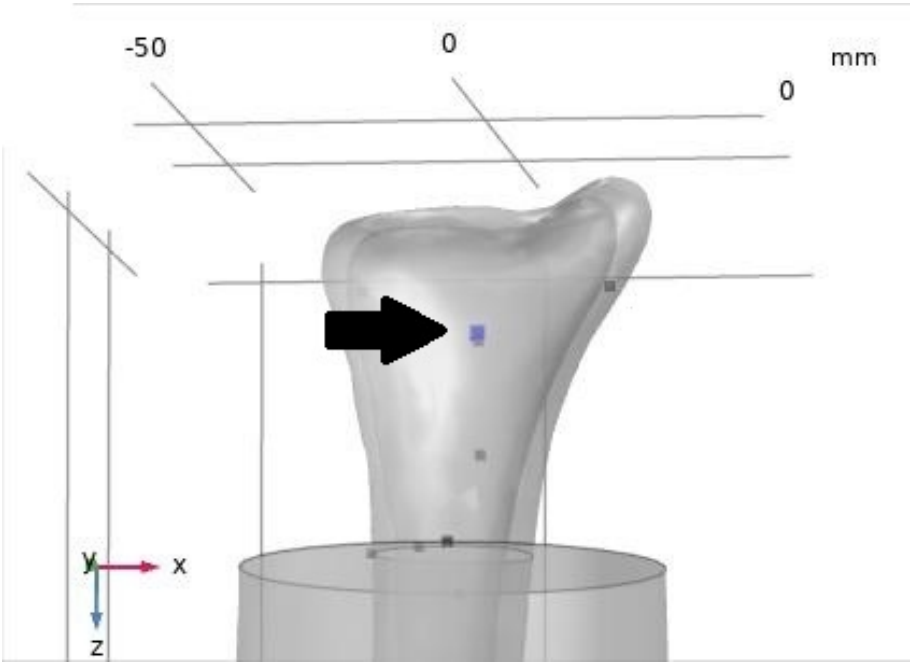

Figure 3.5: Point load for the vertical plane.

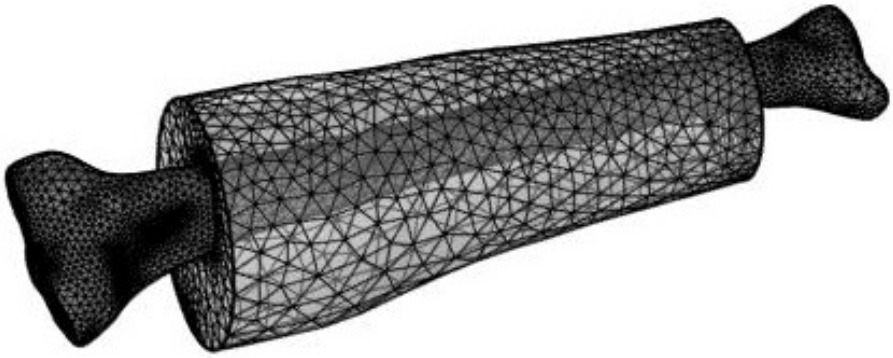

Figure 3.6: Mesh of the model.

It was created a study divided into two steps: eigenfrequency and frequency domain. The number of desired eigenfrequencies is equal to 10 instead for the frequency domain the range selected is (0,15,1500) Hz to highlight the first mode. The resulting mode shapes and the FRF of the model for the driving point will be compared with the experimental results.

4 Results of the dynamic characterization

In this chapter will be presented the results obtained from the experimental tests for the comparison between the different configurations: tibia, tibia surrounded by soft tissues with and without the external fixation.

4.1 Evaluation of the frequency response function

In a general way the results of the modal analysis allow to design the structural system from noise and vibrations applications.
The frequency response function (FRF) is a function used to quantify the response of a system to an excitation, normalized for the magnitude of this last, in the frequency domain. From the FRF is possible to determine the modal parameters: modal frequency, modal damping and mode shape. These lasts are evaluated from a set of frequency response measurement between a reference point, called the degree of freedom (DOF), and a number of measurement points. From the plot of the FRF is possible to see some peaks which represent the natural frequencies where a deformation pattern exists [25]. The FRF, seen as the the transfer function evaluated along the jω-axis in the s-plane, is:

$$FRF = H(\mathrm{j}\omega) = \frac{S_{(x,f)}(\mathrm{j}\omega)}{S_{(f,f)}(\mathrm{j}\omega)} \tag{1}$$

- $S_{(x,f)}(\mathrm{j}\omega)$: average cross power spectrum between output and input
- $S_{(f,f)}(\mathrm{j}\omega)$: average auto power spectrum of the input
- jω: frequency variable

The operating data are vibrations acquired without the excitation forces, so it is considered the response of the system and not the input or the FRF. In this case there is the response of a system to one particular frequency, a linear combinations of all the possible modes for the total response.
A vibration shape determines the magnitude and the phase of the motion connected to one DOF in relation to the other DOFs. In other words a DOF can be defined as

a vector with a position and a direction. If are considered magnitudes and phases of two or more DOFs of operating data is possible to determine the operating deflection shape (ODS). An ODS defines the relative motion between different DOFs and can be derived for one specific frequency. Practically it is the deflection of a structure to a particular frequency. A single degree of freedom (SDOF) model is linear; instead the superimposition of more SDOFs (Fig. 4.1) can develop a multiple degree of freedom model (MDOF) that have more non linearity and is more diffused (Fig. 4.2). The frequency measurement accuracy depends on the frequency resolution of the analysis, it means that if the frequency range is smaller the accuracy is higher [26].

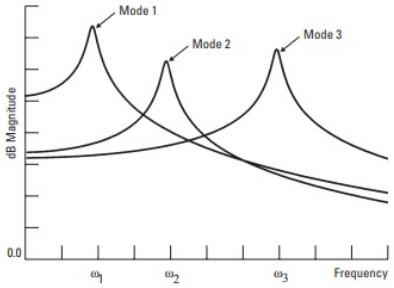

Figure 4.1: Multiple modes for SDOF.

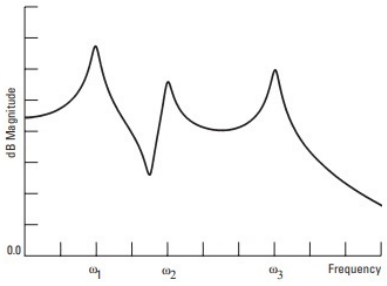

Figure 4.2: MDOF frequency response.

An important properties is that the mode of vibration can be excited in every point of structure other than at nodes of vibration where there is no motion. So the frequency and the damping are global properties of the structure. Instead the mode shapes are influenced by the point of application, scaling and sorting factors because each modal coefficient has a local property. They do not depend on the force applied to the structure and are defined only for linear and stationary motion, instead of the ODS that are influenced by the loads for a non linear and non stationary structure. A curve fitting technique allows to obtain the modal parameter from the FRF associated to the system. It is divided into three steps: determination of how many modes into the data, estimation of a pole and residues for each mode. The dynamics

of the modes can be described by the linear differential equation of the motion:

$$[M]\ddot{x}(t) + [C]\dot{x}(t) + [K]x(t) = 0 \tag{2}$$

with:

- $[M], [C], [K]$= matrices with constants
- $\ddot{x}$= vector for the acceleration
- $\dot{x}$= vector for the velocity
- x= vector for the displacement

In case of a system with simple geometry and homogeneous properties the modes can be found also as a solution of the wave equation. The previously equation (2) confirms the Newton's Second Law in which the internal forces are the mass (internal), the damping (dissipative) and the stiffness (restorative). The cause of the resonant vibration are the mass and the stiffness. For the resolution of the equation (2) is necessary to rewrite it through the Fourier transform:

$$[B(j\omega)][X(j\omega)] = 0 \tag{3}$$

with:

- $[B(j\omega)] = [M](j\omega)^2 + [C](j\omega) + [K]$ the system matrix
- $[X(j\omega)]$ the Fourier transform vector for displacements

The solution of the equation (3) is a set of eigenfrequencies and eigenvalues. The eigenvalues are complex conjugate pairs with modal damping as real part and modal frequency as imaginary part. Each eigenvalue has an eigenvector associated. In more details, a complex conjugate pair of eigenvalues defines a mode, instead, each eigenvector represents a mode shape. The changing into the matrix of the (2) influences also the changing into the boundary conditions and into the modes. The

relationship between modal parameters and the measurement (FRFs) is:

$$h_{i,j}(j\omega) = \sum_{k=1}^{N} \left(\frac{r_{ijk}}{j\omega - \lambda_k} + \frac{r^*_{ijk}}{j\omega - \lambda^*_k} \right) \tag{4}$$

where:

- $h_{i,j}(j\omega)$ is the FRF between the response i and the reference j
- N is the number of the vibration modes that contribute to the dynamic response of the structure into the considered frequency range
- r_{ijk} is the residue value for mode k
- λ_k is the pole value for mode k
- ω is the modal frequency for mode k
- * is used for the comples coniugate
- j is for the imaginary operator

So, at the base of the modal testing there is the measurement of the ODS that is completely arbitrary and can be used for non linear and time varying motion. An ODS can be defined also for structure non resonating. The final post processing allows to obtain modal parameters [25].

4.2 Comparison of the FRFs measurement

During experimental tests the range of frequencies is between 0 and 2048 Hz, with the bending modes frequencies around 200 and 2048 Hz. The resulting plots are amplitude as a function of the frequencies.

4.2.1 Tibia FRF

The first test consists on the tibia excited by a micro hammer. The excitation was done always into the anterior face of the distal epiphysis near the tibial medial

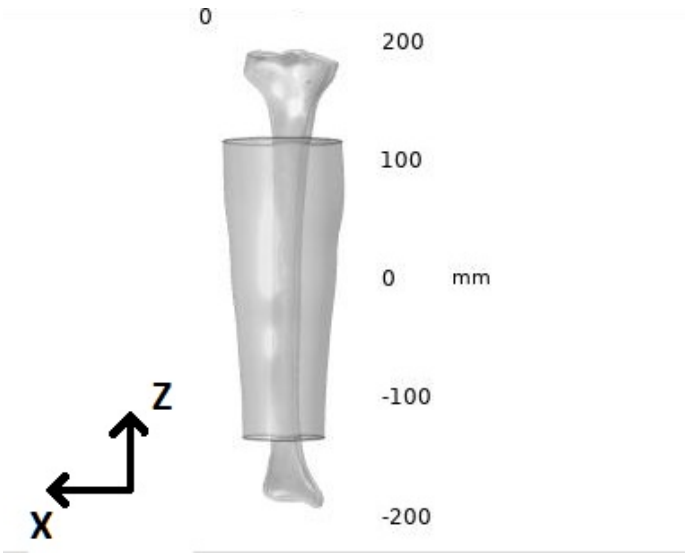

Figure 4.3: Horizontal plane from Comsol reference system.

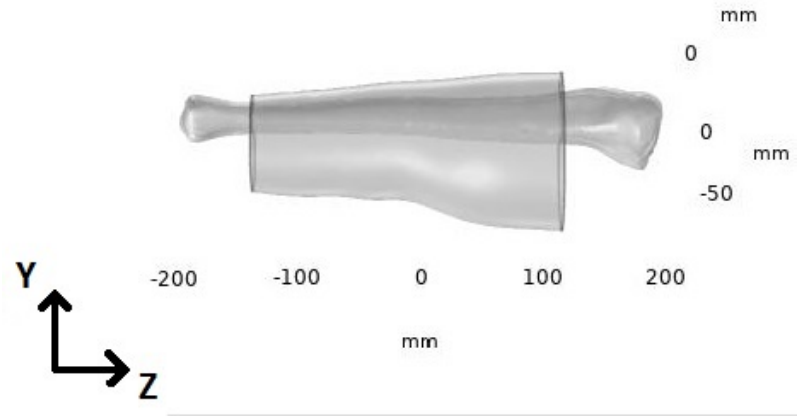

Figure 4.4: Vertical plane from Comsol reference system.

malleolus in horizontal (ZX reference system from Comsol fig.4.3) and vertical (ZY reference system from Comsol fig. 4.4) plane.

Then the output is measured in 4 different points along the surface of the model. The results obtained for the point 1 are shown in figure 4.5 and 4.6.

As seen into the figures the first bending mode occurs into the range 300-500 Hz, instead in the case of the second is between 1000-1300 Hz. Into the table 1 are written in more details the resonant frequencies associated to the bending modes.

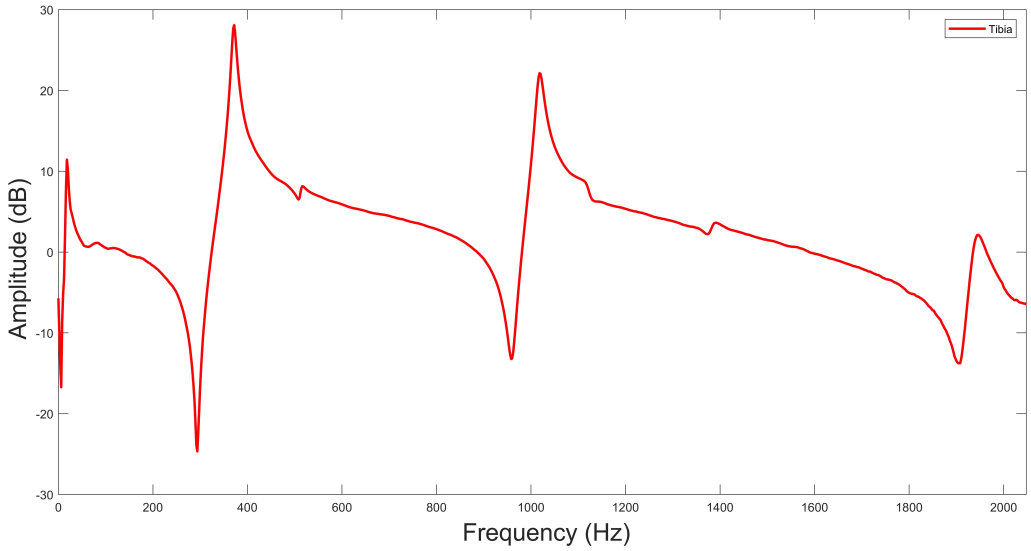

Figure 4.5: Point 1 horizontal plane.

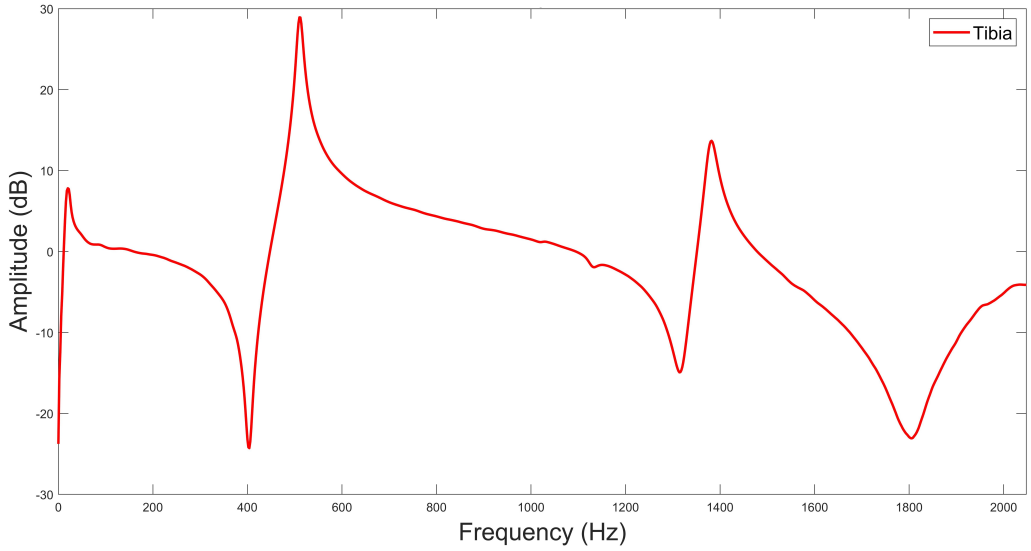

Figure 4.6: Point 1 vertical plane

Table 1: Experimental resonant frequencies in the point 1 for the tibia.

Modes	Horizontal	Vertical
Mode 1	376 Hz	512 Hz
Mode 2	1026 Hz	1384 Hz

4.2.2 FRFs comparison of tibia and tibia with soft tissues

The application of the silicon highlights a damping effect on the results of the bending modes in both planes (Fig. 4.7 and 4.8). The signal is shifted downwards and the peak width is increased due to the damping effect of the material. The resonant frequencies values into the table 2 suggest that the shift into the vertical plane is higher than the horizontal. This is in line with Tsuchikane et al. [14] in which the

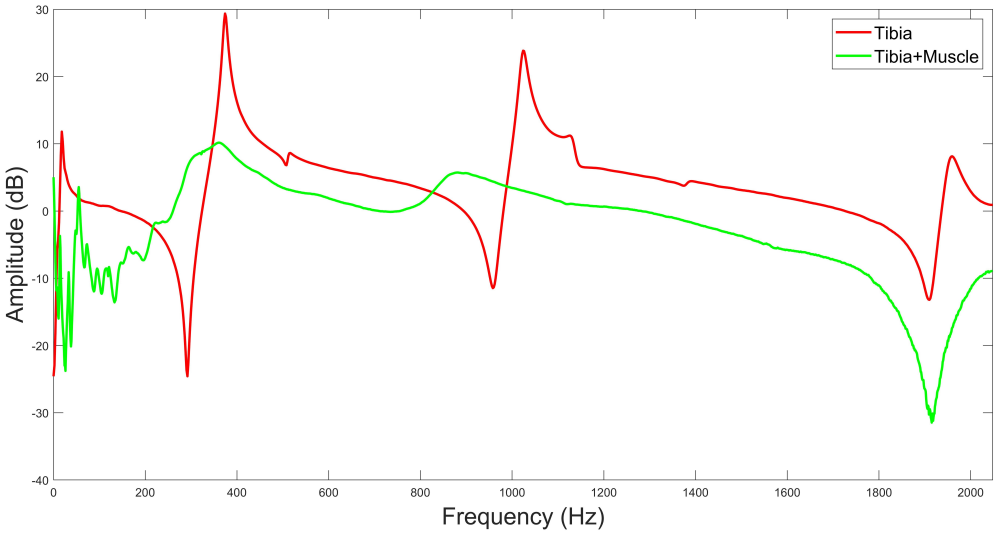

Figure 4.7: Point 1 comparison in horizontal.

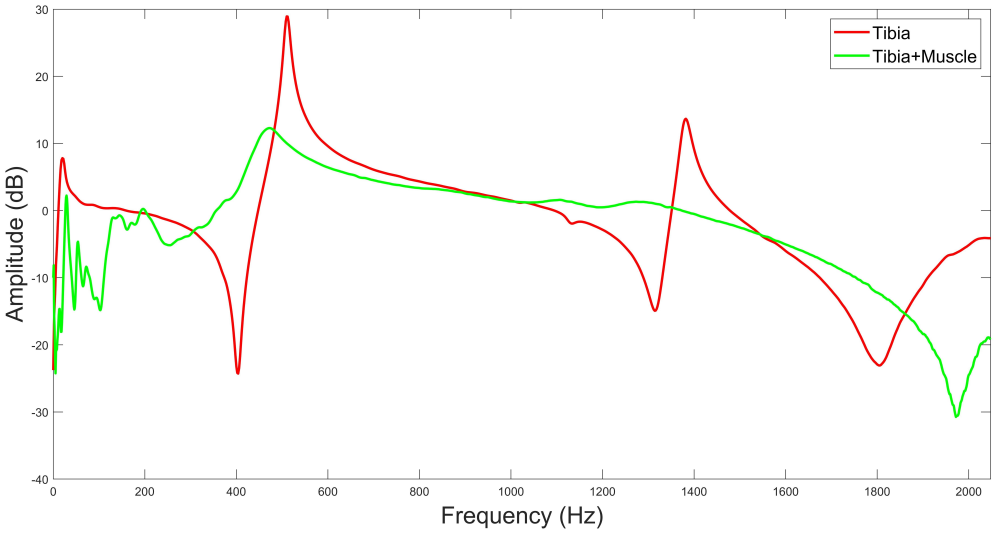

Figure 4.8: Point 1 comparison in vertical.

removal of skin and muscles means an increasing in resonant frequencies (Fig. 1.22).

Table 2: Resonant frequencies in the point 1 for the comparison between tibia and tibia surrounded by soft tissues.

Modes	**Tibia**		**Tibia+Soft Tissues**	
	horiz.	vert.	horiz.	vert.
Mode 1	375 HZ	512 Hz	362 Hz	474 Hz

4.2.3 FRFs comparison between tibia with and without external fixation

Adding the external fixation causes a structure more rigid than that characterized only by the silicon. The figures 4.9 and 4.10 show the comparison between these two systems in horizontal and vertical plane. In the horizontal plane, in presence of the fixation, is possible to see an upwards shift of the signal due to the structure more rigid and to an increasing in the mass. Another effect is the decreasing in the width of the peak. Instead, into the vertical plane the resonant frequencies do not change a lot, however there is also a decreasing into the width of the peak. From the table 3 is highlighted how the most relevant shift in frequency for the first bending mode

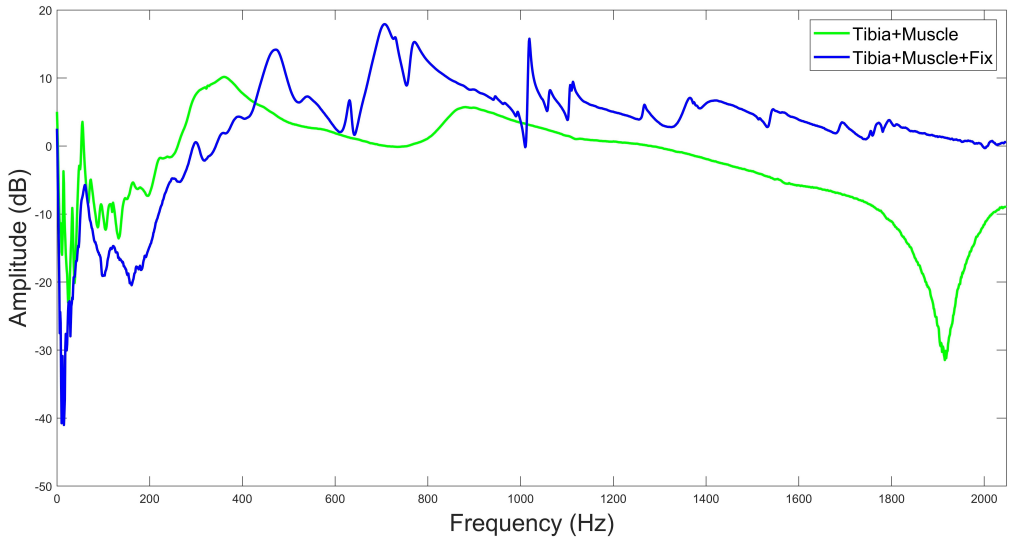

Figure 4.9: Point 1 in horizontal: comparison of tibia surrounded by soft tissues with and without external fixation.

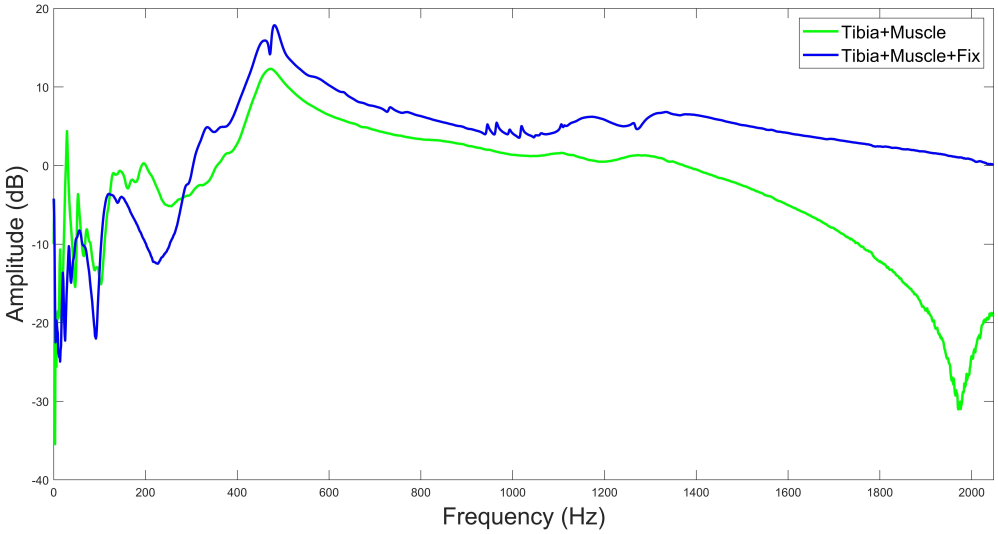

Figure 4.10: Point 1 in vertical: comparison of tibia surrounded by soft tissues with and without external fixation.

is in horizontal. In vertical the shift is not so relevant.

Table 3: Resonant frequencies in the point 1 for the comparison between tibia and tibia surrounded by soft tissues.

Modes	**Tibia+Soft Tissues**		**Tibia+Soft Tissues+Fixation**	
	horiz.	vert.	horiz.	vert.
Mode 1	362 HZ	474 Hz	473 Hz	482 Hz

4.2.4 FRFs and mode shapes from numerical model

The numerical model of the tibia including soft tissues, under the hypothesis of an isotropic silicon, gives two different results in horizontal and vertical plane.
The study results, into horizontal plane for the driving point, give a FRF shown into the figure 4.11. It is possible to observe the arising of first mode around 360 Hz with a first maximum peak. Because of the silicon effect at higher frequencies is not possible to see other peaks. Anyway in this case the attention is focused on the first mode. From the comparison with the experimental FRF (highlighted in red) it is possible to see as, without the damping effect into numerical model, not all

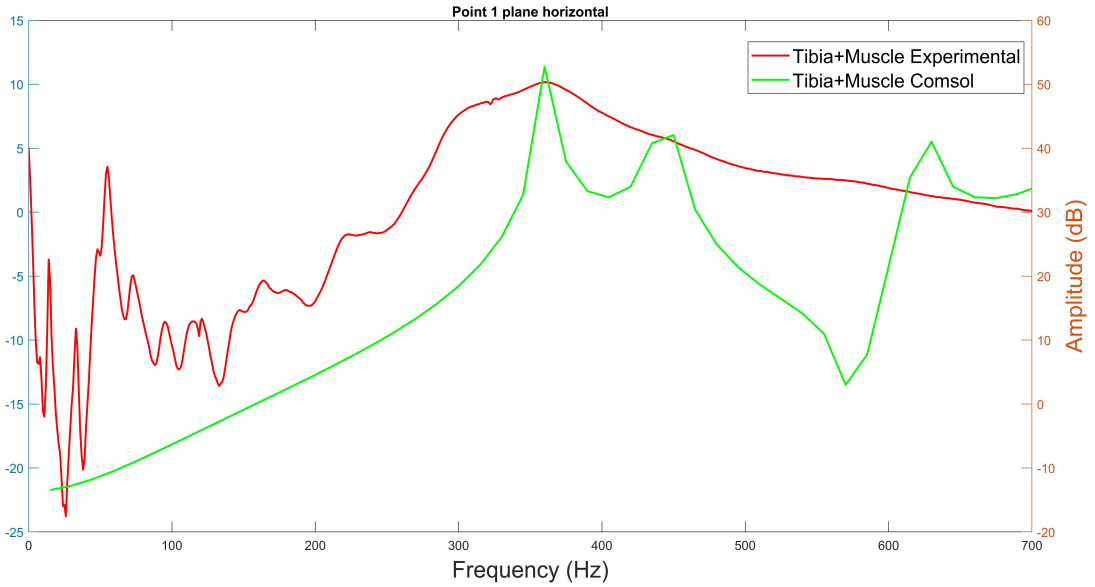

Figure 4.11: Point 1 in horizontal from numerical model of tibia including soft tissues.

the peaks are visible. At same time into experimental part, because of the damping effect, a double peak is depicted as only one.

The mode shape obtained for a frequency of 360 Hz is shown in the next plot (fig. 4.12) , which shows tibia displacement in presence of the adding mass. On the right (fig. 4.13) is represented the first mode for the horizontal plane obtained from numerical model in Verdenelli et al. study [18]. It can be observed that including soft tissues in modal shape there is an influence due to rigidity higher than that of adding mass.

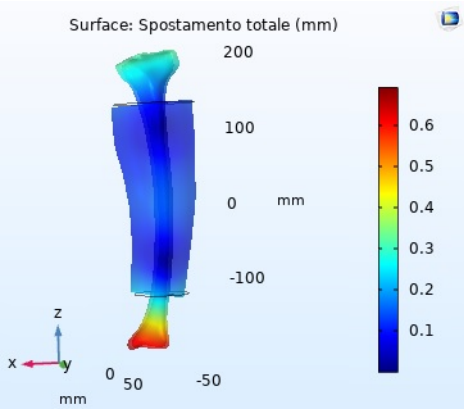

Figure 4.12: Mode shape at 360 Hz in horizontal plane.

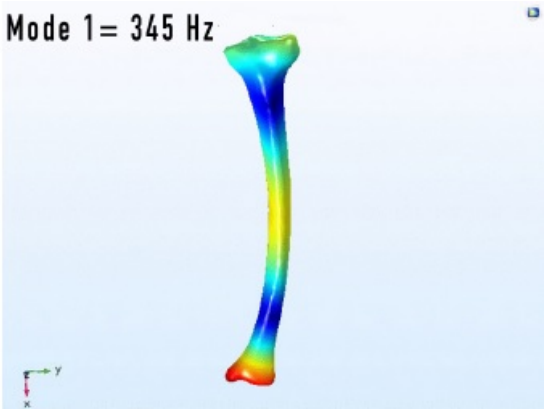

Figure 4.13: Mode shape from Verdenelli et al study [18]

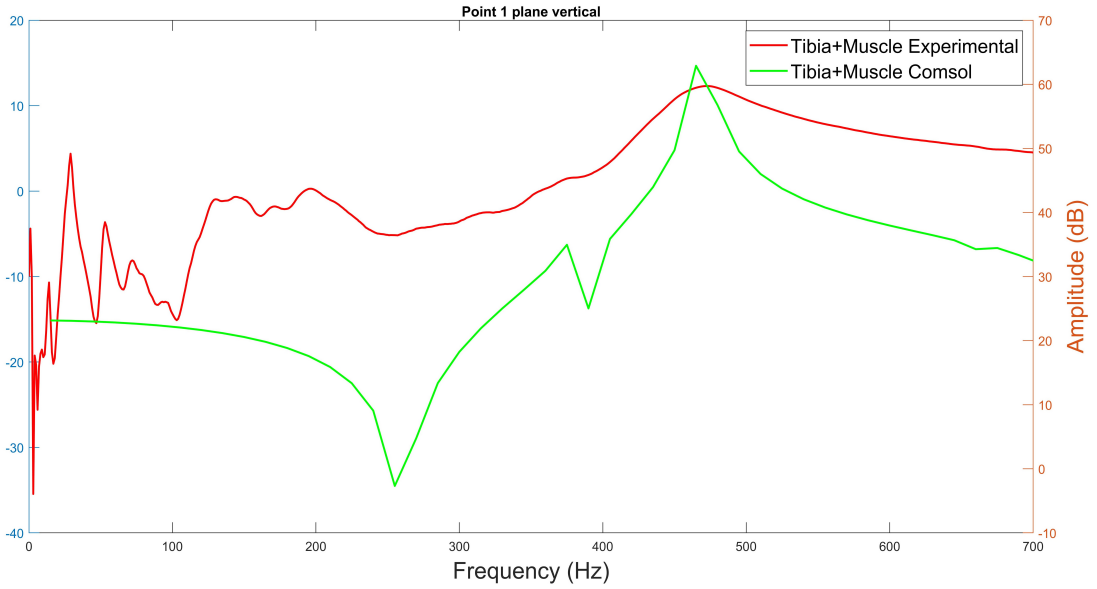

Figure 4.14: Point 1 in vertical from numerical model of tibia including soft tissues.

In vertical plane there is a maximum peak for the first mode at 465 Hz (Fig. 4.14) with a mode shape at the same frequency represented in figure 4.15. From mode shape of the previously study (fig. 4.16) it possible to see same shape but reached at higher frequency.

From previously results is possible to see how the numerical model is in line with what obtained from experimental test. Mode shapes highlight the rigidity of the model due to the adding silicon mass with a displacement lower than the case of the only tibia.

In table 4 are shown frequencies for experimental test and numerical model. It can be observed some differences that are higher into the horizontal plane. One limitation is represented by the difficulty into realization of boundary condition. However this numerical model can be validated as a good model to predict the behaviour of the tibia including soft tissues under impact hammer excitation in both planes.

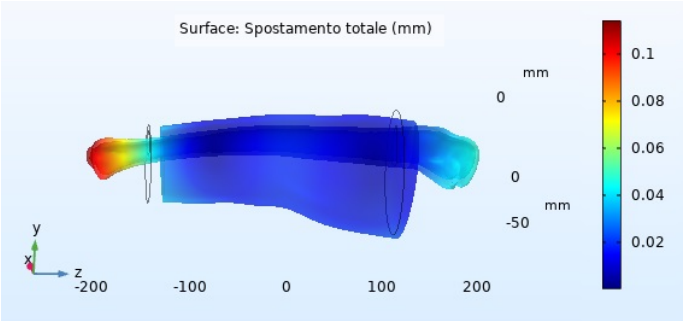

Figure 4.15: Mode shape at first mode in vertical plane (480 Hz).

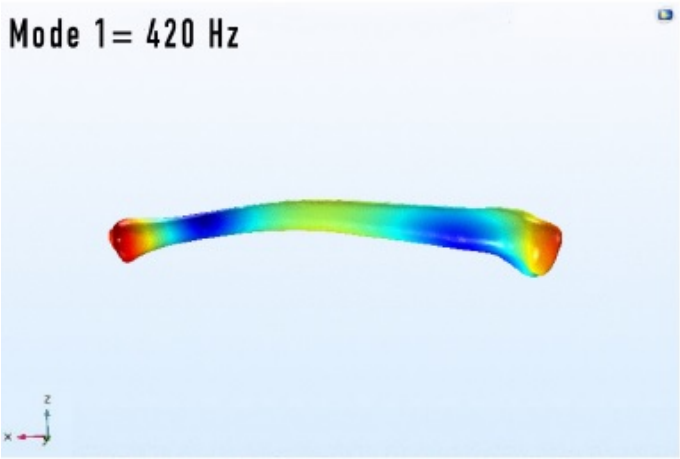

Figure 4.16: Mode shape from Verdenelli et al study [18]

Table 4: Resonant frequencies in the point 1 for tibia including soft tissues: comparison between experimental and numerical model results.

Modes	**Experimental**		**Numerical model**	
	horiz.	vert.	horiz.	vert.
Mode 1	362 HZ	474 Hz	360 Hz	465 Hz

5 Fracture healing curve

The healing fracture curve is obtained following the steps described into the Ong et al.[15] work, based on the evaluation of the transfer function (TF) between input and PVDF output:

$$TF(f_i) = \frac{V_{inputforce}(f_i)}{V_{PVDF}(f_i)} \tag{5}$$

The healing index is derived from the difference between the TF in the minute x and the same at the starting time of the experiment.

$$TF_{change}(f_i) = |TF_{t=xmin}(f_i) - TF_{t=0min}(f_i)| \tag{6}$$

Spikes and changes are smoothed out through a window of 10 Hz. The healing curve is the result of the cumulation of the windowed function:

$$TF_{windowed}(f_i) = \int_{f_i}^{f_i+10} TF_{change}(f_i)df \tag{7}$$

$$HealingIndex = \sum TF_{windowed}(f_i) \tag{8}$$

Into the figure 5.1 is drawn an example of fracture healing curve. Non union or delayed union is depicted by the differentiation respect time of the healing index. Ong et al. analyses the index in case of addition to a clay simulating the muscle

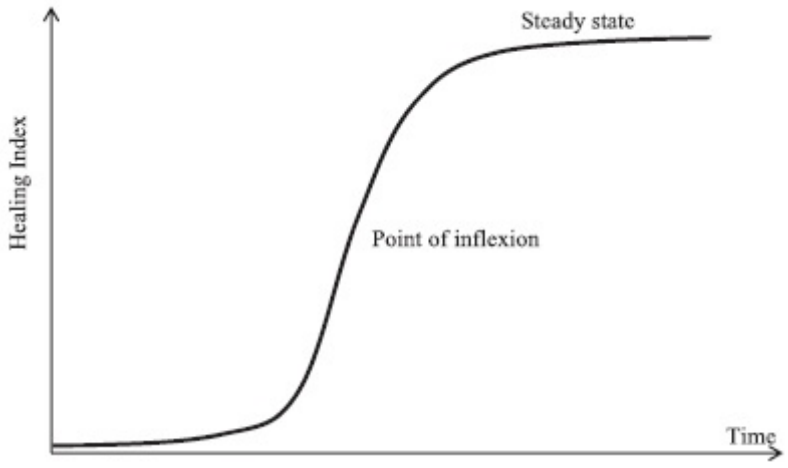

Figure 5.1: Fracture healing index profile.

around the tibia. This last situation does not influence the profile of the healing index curve that can monitor epoxy curing [15].
As confirmed by Chiu et al. [27] the presence of the adding mass, simulating the soft tissues, does not influence the state of healing assessment in a fixated femur.

5.1 Experimental test

The tibia shaft fracture is simulated through a transverse cut of 2 mm done with a handsaw (Fig.5.2). The bone is excited by shaker into the pin before fracture and is measured with two accelerometers applied, one into the same pin of the excitation and another into pin just after the fracture. The bone callus is simulated with X-60 bicomponent cement which is preferred than glue for its ability to reach high rigidity similar to the material of tibia in a short time of hardening (Fig. 5.3).
The pin is excited through an aluminium cylinder which encloses the top head of the pin. The random excitation can be more invasive because of the continuously excitation of the pin; instead the burst random signal is less invasive because of the lower duration. For the healing index curve is extracted the single burst from the accelerometer's signal before and after the cut and is plotted relative to time the Root Mean Square (RMS) computed. From the RMS points is fitted a curve through a cubic polynomial.
At time 0s the fracture is filled with the X-60 which reaches the rigidity of the hard bone callus in 180s representing the end of the reparation phase. At time 60s starts

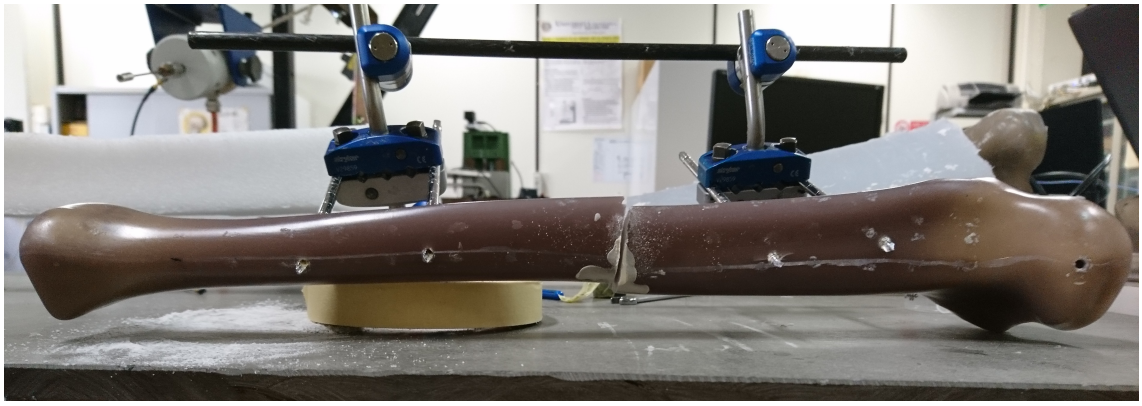

Figure 5.2: Tibia with shaft fracture.

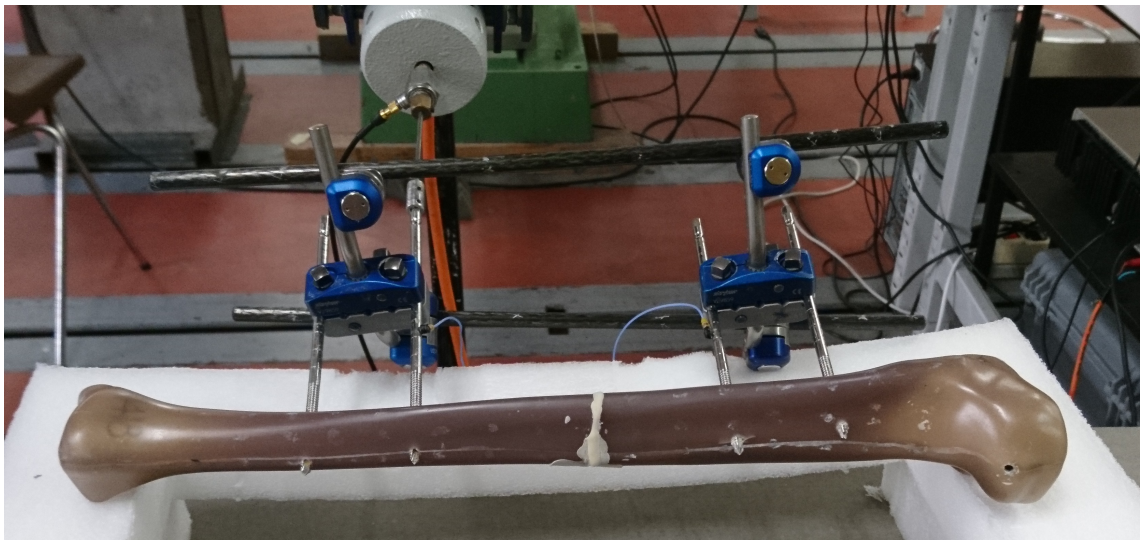

Figure 5.3: Tibia with bone callus.

the biological process for the soft callus formation.

5.2 Healing curve obtained

In the resultant curve of the tibia without silicon is distinguishable the healthy curve that is constant in time from the fractured one which has an asymptotically behaviour before reaching the healthy curve, confirming the results of Ong [15].

From the figures 5.4 and 5.5 are highlighted some differences. First of all the shape

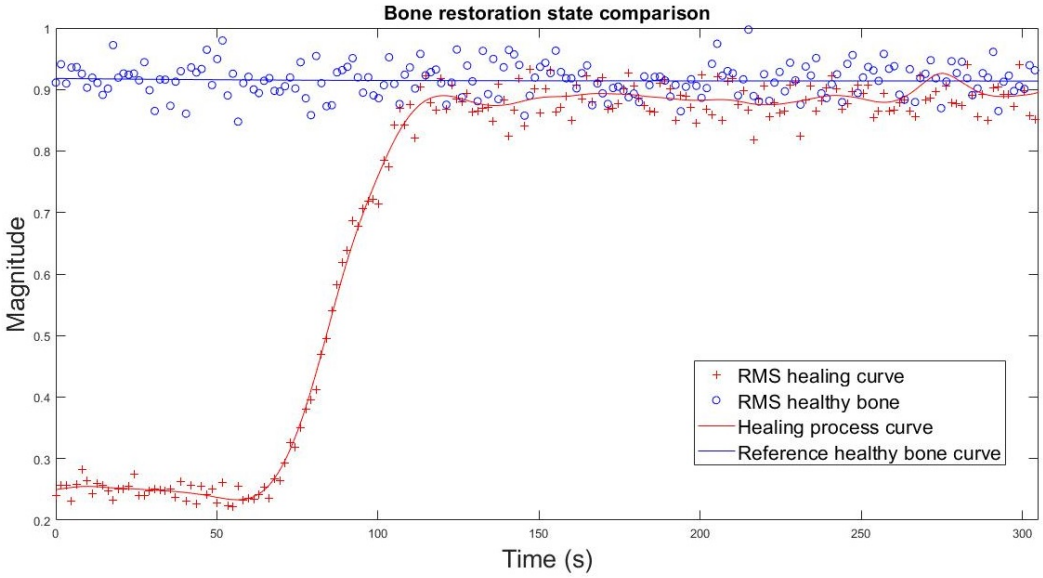

Figure 5.4: Bone restoration curve calculated in July 2018.

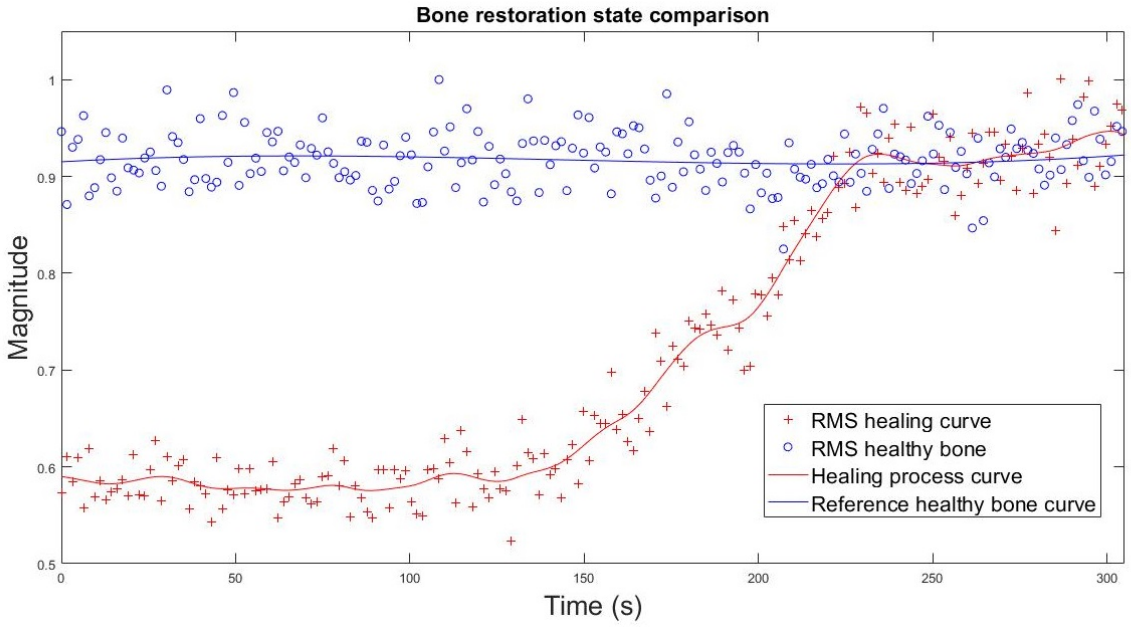

Figure 5.5: Bone restoration curve calculated in September 2019.

that is sigmoid into the first and more linear into the other one. Tibia fractured in 2019 presents a delay into reaching the healthy line and a lower distance between lines before healing process. Another effect is the higher amplitude after the end of the healing process. Also the curve rate of growth is different. All these negative

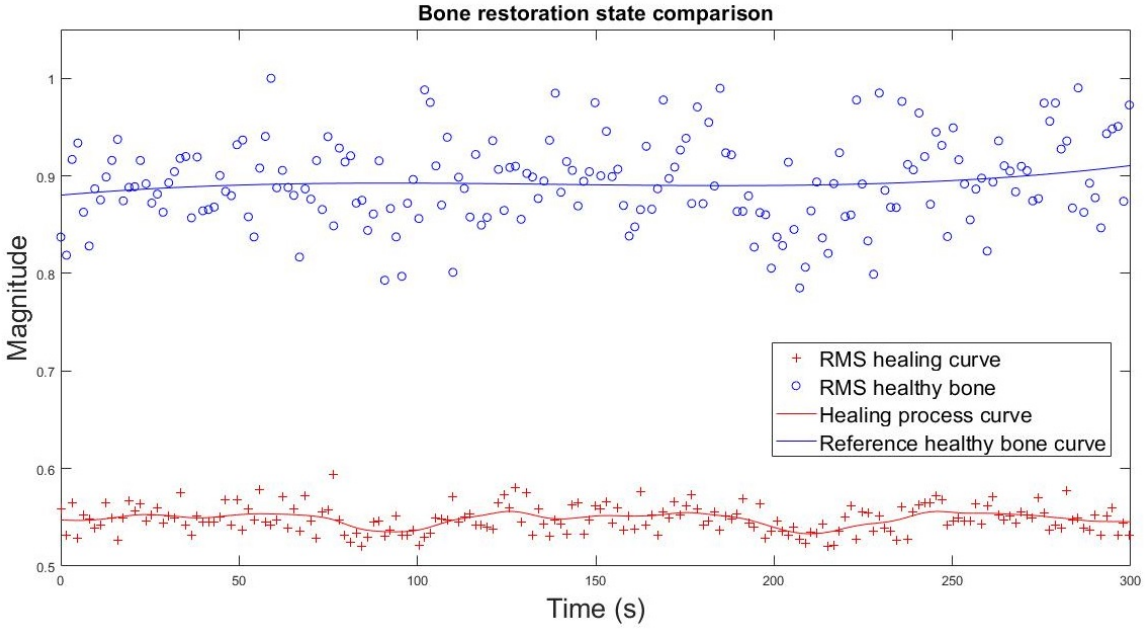

Figure 5.6: Healing curve of the tibia surrounded by soft tissues before X60 filling.

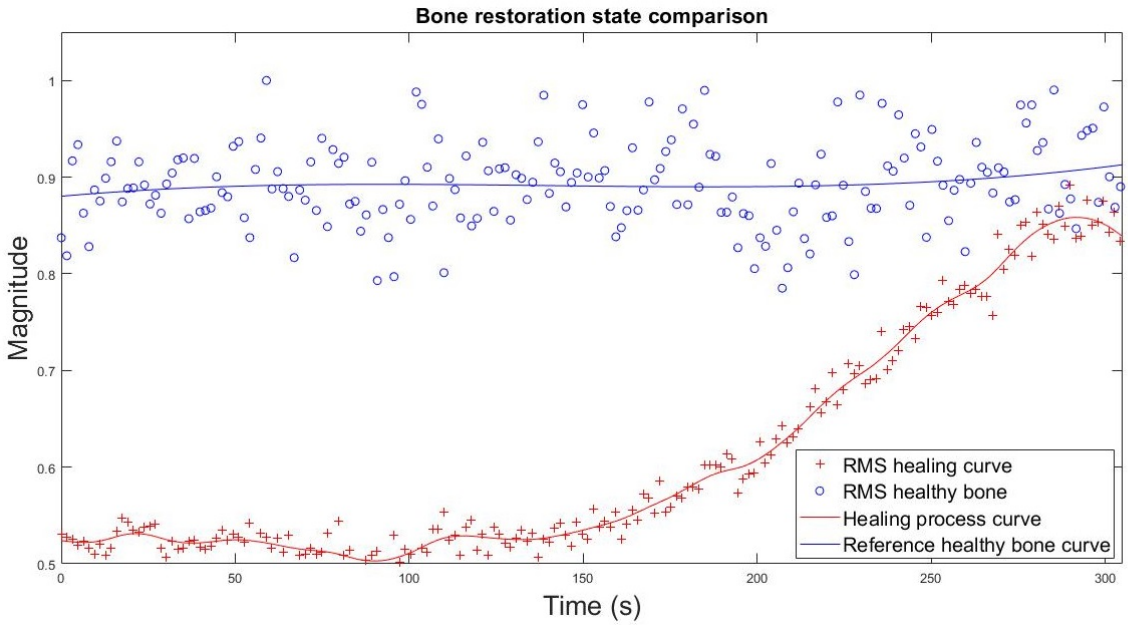

Figure 5.7: Healing curve of the tibia surrounded by soft tissues with X60.

aspects can be connected to the remained X60 from the previously experiment. The figure 5.6 compares the healing curve in case of the fracture, before filling with X60, to distinguish healthy from fractured. In the same way, with the handsaw is realized the cut of the tibia surrounded by silicon and then is filled with the X-60. It is visible how the healthy curve is maintained parallel respect that of the case with the cut. Instead the comparison before and after the cut highlights a behaviour similar to the tibia without the silicon (Fig. 5.7). The difficulty into reaching the healthy curve can be connected to the fact that the silicon does not allow the X60 to fill the entire fracture into the bone in a similar manner of the "free" tibia. A little shift is also present at level of the magnitude due to the presence of the silicon around the tibia.

Into table 5 there is an overview of numerical number from the healing curves

Table 5: Comparison of numerical values obtained from healing curves.

Values	**Tibia 2018**	**Tibia 2019**	**Tibia+Silicon 2019**
Distance h/f	0.67±0.0086	0,33±0,0095	0.37±0.0121
Starting time	60 s	120 s	130 s
Interval	60 s	110 s	160 s

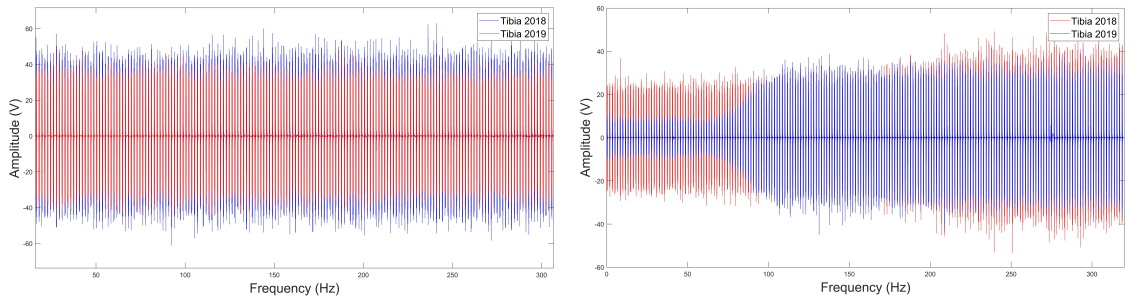

(a) Second pin. (b) Third pin.

Figure 5.8: Measurement in the pins during healing process. Blue: Tibia 2018. Red: Tibia 2019.

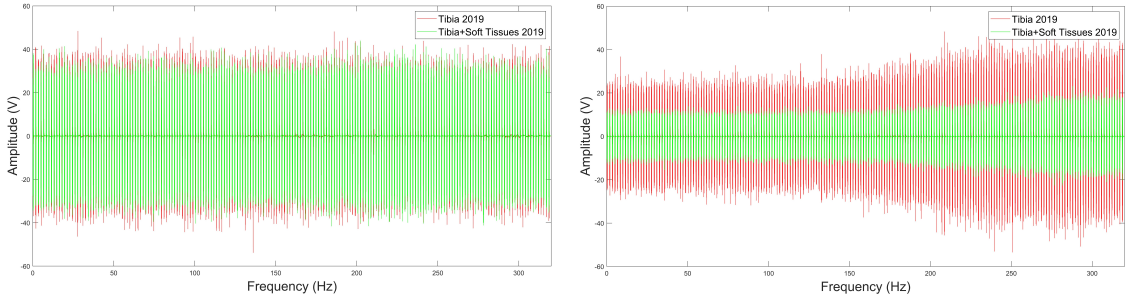

(a) Second pin. (b) Third pin.

Figure 5.9: Measurement in the pins during healing process. Red: Tibia 2019. Green: Tibia+Soft Tissues 2019

in order to compare the difference from each experimental test and to confirm the difficulty in doing repeatability. In particular is analysed distance between healthy/fractured line before healing process, time for healing process starting and interval of time to reach the healthy curve.

Figures 5.8a and 5.8b show measurements at level of the external fixation's second and third pin during healing process. The blue signal is for tibia in July 2018, instead the red one is for tibia in September 2019. The signal amplitudes are lower in the new measurements and do not increase a lot after bone callus formation. Into second plots (Fig. 5.9a and 5.9b) green signal is for tibia surrounded by soft tissues. Including silicon the amplitude in third pin is maintained lower also after healing process. This is an additional proof that the signals acquired after more than one cut are less accurate and do not allow the repeatability of the experiment on the same model. It highlights, also, the difficulty with adding mass into simulating the

bone callus formation.

5.3 FRF measurement into the pin

In this section the attention is on the results came from the FRF measured at level of the second accelerometer on third pin, located after the shaft fracture. Comparing the FRF, before and after the cut, are present some differences. First of all, the curve acquired from the tibia in July 2018 (fig. 5.10) is characterized by peaks, before and after the cut, at different amplitude but with same shape at low frequencies. Instead at higher frequency both amplitude and frequencies are shifted. In July 2019 (fig. 5.11) some peaks are lost, also, at low frequencies and signal is more affected by noise.

This could be connected to the difficulty into removing all the X60 remained from the previously experiment. The additional X60 do not attach in a good way on the X60 remained from the previously test and the one used to cover the empty region of the tibia which reproduces the medullary canal. Another influential factor is the free-free boundary condition between the tests in 2018 and 2019.
A different behaviour is confirmed also by the cut of the tibia in September 2019 (fig.

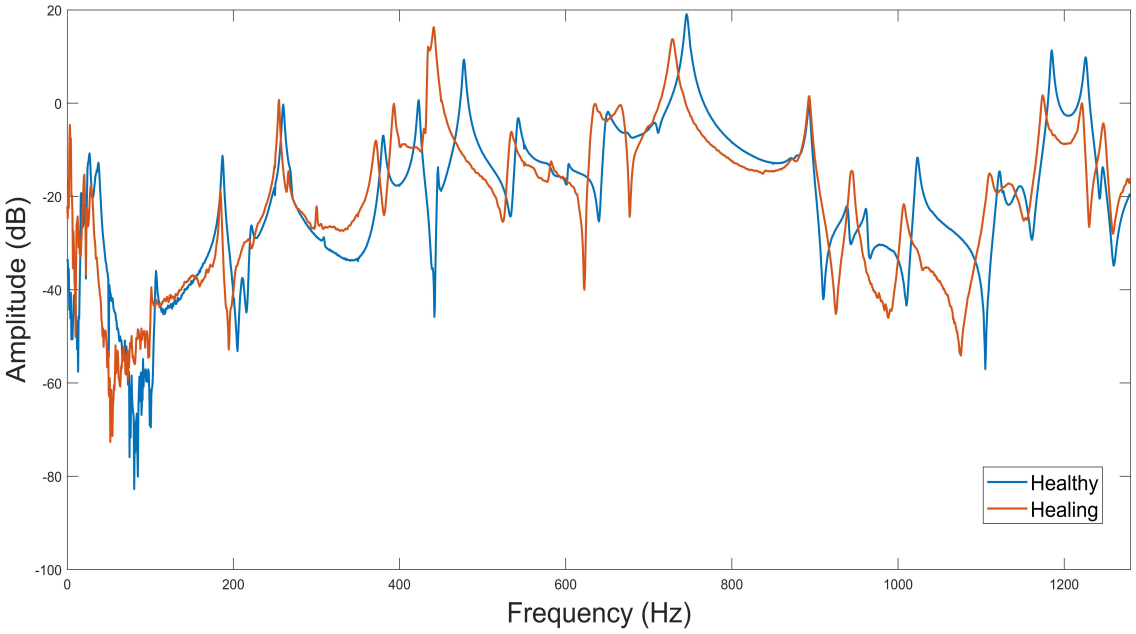

Figure 5.10: FRF of third pin in tibia (July 2018).

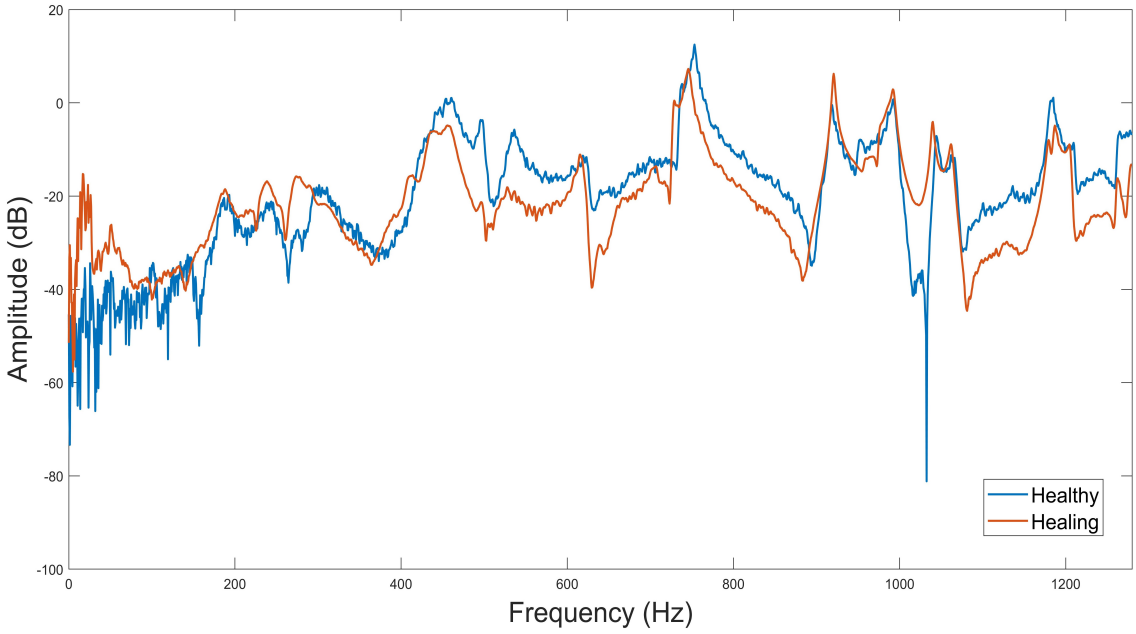

Figure 5.11: FRF of third pin in tibia (July 2019).

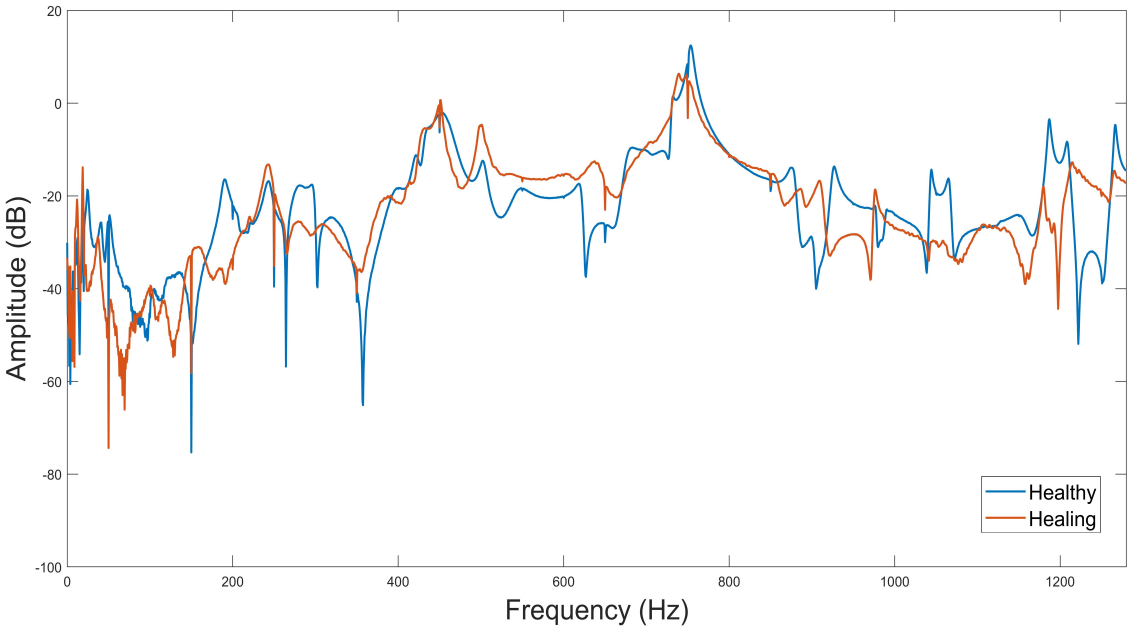

Figure 5.12: FRF of third pin in tibia (September 2019).

5.12) compared to July 2019. Here into middle frequencies the behaviour is similar with some changes in amplitude instead at low and high frequencies the shape is lost. In this last case the reason could be connected to the temperature hotter in July. A suggestion, for further studies, could be to acquire signal into same thermal conditions.

The FRF of the tibia surrounded by soft tissues is characterized by peaks at the same frequencies with only a downwards shift in amplitude. The adding silicon mass has a damping effect which reduces the perception of the cut than the case of the only tibia. A relevant difficulty is the total filling of fracture with the X60 for the presence of adding material. Furthermore, the tibia surrounded by soft tissues is maintained fixed by the external fixation and by the silicon, instead of the tibia only by the fixation.

Into last plot (fig. 5.13) there is a comparison between healthy tibia in 2019 with and without soft tissues. The red shape, for tibia including soft tissues, is different and has a lower amplitude.

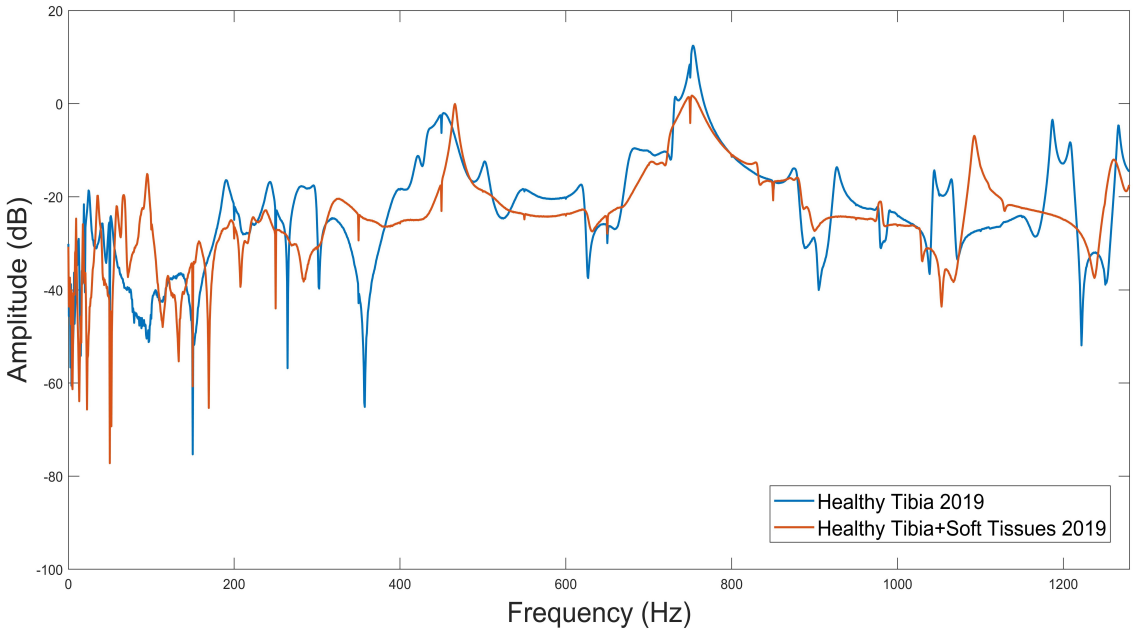

Figure 5.13: Comparison between FRF of healthy tibia in 2019 and healthy tibia including soft tissues.

Conclusions

This work is focused on a complex structure characterized by a human tibia at which is added a mass of silicon simulating soft tissues. The system is undergone to vibrations in order to analyse its behaviour.

The first part of the experiment is based on the direct excitation of the bone shaft by a hammer and the recording through an accelerometer. The FRF obtained came from the tibia, tibia adding soft tissues with and without external fixation. Adding mass causes a downward shift of the resonant frequencies into first mode of 3.5% in horizontal and of 7% in vertical plane. The peak width is increased due to the damping effect of the material as seen in Tsuchikane study [14].
Adding external fixation into the bone, surrounded by soft tissues, presents an increasing in the structure rigidity and in mass. As a consequence the resonant frequencies are higher with a relevant effect into horizontal plane (around 30%) respect the vertical (2%) and a decreasing into width of peaks.
Starting from the 3D tibia model and by the soft tissues model, measured from the reality, it was realized a numerical model to predict and to evaluate the bone behaviour under excitation on the shaft. This model can be validated because its results are similar with what obtained by the experimental tests, both in horizontal and vertical plane under hypothesis of isotropic silicon. From mode shapes obtained is possible to see how the added mass limits displacement of entire system and how at higher frequencies there is a damping effect which causes a linear shape of the FRF.

The second part of the work, using as reference the Ong study [15], evaluates the index healing curve in different configurations. For the experimental test the tibial shaft is fractured by a cut of 2 mm with a handsaw and the bone callus phases are simulated by a bi-component glue. In this case the pins of the fixation are used as a transmission medium and the shaker is used as input excitation. The cement reproduces in a good way the biological process.

Comparing the index curve healing from the previously year with what obtained from this year it is possible to see a delay into starting point for bone callus formation and a longer interval of time for the healing process. The distance between the line for the healthy and fractured bone is lower. These results are, also, confirmed by the FRF measured by accelerometer before and after healing process. In particular is not possible to see a relevant increasing into amplitude, as a function of time, to distinguish the soft from hard bone callus formation. After more than one cut, signal presents a different behaviour.

Results from the first part confirms that adding soft tissues and external fixation influence resonant frequencies and the shape of the modal analysis in case of a healthy tibia.
All the considerations from second part highlight lack of repeatability in the experimental tests after more than one cut. For this reason is validated a numerical model for tibia including soft tissues which predicts bone behaviour. For the silicon of the model is not considered the damping effect, so, some peaks are lost at lower frequencies and the peak at the experimental resonant frequencies have a marked shape. The modal shapes occur at frequencies higher than the case of the only tibia. It means that into model with silicon the influence of rigidity is higher than that of the mass. It represents a starting point for future studies in which will be added also the external fixation.
The most relevant negative effect is due to cement, remained from the previously cut, which increases local rigidity and decreases rate for healing process. Amplitude of healthy line is reached with a delay in time, starting from a higher value of amplitude and with a different shape of the curve. Another influence is connected to the temperature and humidity at which the experiment takes place, results obtained in July are not comparable with that ones in September. A suggestion for experimental part is to maintain the same thermal condition.

Starting from the validated numerical model, further studies are necessary, to add also the external fixation, to improve the constraint conditions and to add the

material damping effect. The future goal is to have a complete numerical model to obtain faithful resonant frequencies and modal parameters overcoming difficulties into repeatability of experimental tests during fracture simulation.

References

[1] J. Betts, P. Desaix, E. Johnson, J. Johnson, O. Korol, D. Kruse, B. Poe, O. College, J. Wise, M. Womble, *et al.*, *Anatomy & Physiology*. Open Textbook Library, OpenStax College, Rice University, 2013.

[2] T. Rüedi, R. Buckley, and C. Moran, "Ao principles of fracture management. 2nd expanded ed," *Switzerland: AO Publishing*, pp. 164–166, 2007.

[3] E. Gautier and R. Pesantez, "Surgical reduction," *AO principles of fracture management*, vol. 1, pp. 165–188, 2007.

[4] A. R. Elniel and P. V. Giannoudis, "Open fractures of the lower extremity: Current management and clinical outcomes," *EFORT Open Reviews*, vol. 3, no. 5, pp. 316–325, 2018.

[5] Stryker, *T2 Tibial Nailing System*. Stryker Orthopaedics.

[6] M. Bisaccia, C. I. Vicente, L. Meccariello, G. Rinonapoli, G. Falzarano, G. Colleluori, A. Schiavone, P. Ferrara, R. Pezzella, E. Manzi, *et al.*, "The history of external fixation, a revolution idea for the treatment of limb's traumatized and deformities: From hippocrates to today.," *vol*, vol. 3, pp. 1–9.

[7] S. A. Green, "Complications of external skeletal fixation.," *Clinical Orthopaedics and Related Research*, no. 180, pp. 109–116, 1983.

[8] W. R. Pontarelli, "External fixation of tibial fractures," *The Iowa orthopaedic journal*, vol. 2, p. 80, 1982.

[9] G. Raimbeau, J. Chevalier, and J. Raguin, "Les risques vasculaires du fixateur en cadre à la jambe," *Rev Chir Orthop*, vol. 65, no. Suppl II, pp. 77–82, 1979.

[10] R. K. Lippmann, "The use of auscultatory percussion for the examination of fractures," *JBJS*, vol. 14, no. 1, pp. 118–126, 1932.

[11] N. H. McGaw, "Osteosonometry.," *Arch. Surg*, no. 205, pp. 45–195, 1942.

[12] T. Sekiguchi and T. Hirayama, "Assessment of fracture healing by vibration," *Acta Orthopaedica Scandinavica*, vol. 50, no. 4, pp. 391–398, 1979.

[13] P. Cornelissen, M. Cornelissen, G. Van der Perre, A. Christensen, F. Ammitzbøll, and C. Dyrbye, "Assessment of tibial stiffness by vibration testing in situ—ii. influence of soft tissues, joints and fibula," *Journal of biomechanics*, vol. 19, no. 7, pp. 551–561, 1986.

[14] A. Tsuchikane, Y. Nakatsuchi, and A. Nomura, "The influence of joints and soft tissue on the natural frequency of the human tibia using the impulse response method," *Proceedings of the Institution of Mechanical Engineers, Part H: Journal of Engineering in Medicine*, vol. 209, no. 3, pp. 149–155, 1995.

[15] W. Ong, W. Chiu, M. Russ, and Z. Chiu, "Integrating sensing elements on external fixators for healing assessment of fractured femur," *Structural Control and Health Monitoring*, vol. 23, no. 12, pp. 1388–1404, 2016.

[16] L. Mattei, A. Longo, F. Di Puccio, E. Ciulli, and S. Marchetti, "Vibration testing procedures for bone stiffness assessment in fractures treated with external fixation," *Annals of biomedical engineering*, vol. 45, no. 4, pp. 1111–1121, 2017.

[17] L. Mattei, F. Di Puccio, and S. Marchetti, "Fracture healing monitoring by impact tests: Single case study of a fractured tibia with external fixator," *IEEE journal of translational engineering in health and medicine*, vol. 7, pp. 1–6, 2019.

[18] L. Verdenelli, R. Rossetti, P. Chiariotti, M. Martarelli, and L. Scalise, "Experimental and numerical dynamic characterization of a human tibia," in *Journal of Physics: Conference Series*, vol. 1149, p. 012029, IOP Publishing, 2018.

[19] P. Piezotronics, *ICP® Impact Hammer: Installation and Operating Manual*. PCB Group.

[20] P. Piezotronics, *Piezoelectric ICP® Accelerometers*. PCB Group.

[21] Siemens, *Siemens PLM Software: LMS SCADAS*. Siemens Product Lifecycle Management Software Inc.

[22] Stryker, *Hoffman® II External Fixation System.* Stryker Corporation.

[23] TIRA, *Vibration Test System TV 50009.* TIRA.

[24] O. C. Zienkiewicz, R. L. Taylor, P. Nithiarasu, and J. Zhu, *The finite element method*, vol. 3. McGraw-hill London, 1977.

[25] M. Richardson and B. Schwarz, "Modal parameter estimation from operating data," *Sound and vibration*, vol. 37, no. 1, pp. 28–39, 2003.

[26] A. Technologies, *The fundamentals of modal testing.* Agilent Technologies.

[27] W. K. Chiu, B. S. Vien, M. Russ, and M. Fitzgerald, "Towards a non-invasive technique for healing assessment of internally fixated femur," *Sensors*, vol. 19, no. 4, p. 857, 2019.